Continental Shelf Research ▮ (▮▮▮▮) ▮▮▮–▮▮▮

Contents lists available at ScienceDirect

Continental Shelf Research

journal homepage: www.elsevier.com/locate/csr

The evolution of a thin phytoplankton layer in strong turbulence

Zhankun Wang *, Louis Goodman

School of Marine Science and Technology (SMAST), University of Massachusetts Dartmouth, 706 South Rodney French Blvd, New Bedford, MA 02744, USA

ARTICLE INFO

Article history:
Received 25 November 2008
Received in revised form
16 March 2009
Accepted 3 August 2009

Keywords:
Thin layers
Chlorophyll *a*
Turbulence
AUV
Buoyancy Reynolds number
Turbulent eddy velocity

ABSTRACT

Simultaneous and collocated spatial measurements of turbulence, fine structure, and chlorophyll *a* fields were made from the Autonomous Underwater Vehicle T-REMUS as a part of the Layered Organization in the Coastal Ocean (LOCO) experiment. The T-REMUS was operated in a cycling 5° yo-yo mode. Deployments were of 8 h duration and consisted of a series of across isobath legs, each of 2.5 km in extent. From the suite of sensors onboard the T-REMUS vehicle we are able to measure directly the turbulent eddy velocity, $w_e = \sqrt{\varepsilon/N}$, and turbulent Reynolds number, $\mathrm{Re}_b = (\varepsilon/\nu N^2)$, in the vicinity of a thin chlorophyll *a* layer. Using the turbulent eddy velocity, we develop criteria for when phytoplankton will behave as passive Lagrangian tracers. The turbulent Reynolds number is used as an indicator of turbulence strength, with the criterion of $\mathrm{Re}_b = 200$ the boundary between weak and strong turbulence. We present data for the case of a spatially extensive thin layer being advected into the T-REMUS LOCO site. Using the above criterion, we observe that thin chlorophyll *a* layers can exist and be embedded as passive Lagrangian tracers in both weak and strong turbulent conditions. During a time period of weak turbulence $\mathrm{Re}_b < 200$ little diffusion occurs and the thin layer remains compact. Under strong turbulence $\mathrm{Re}_b > 200$ the thin layer weakens and diffuses as it is advected through the experimental site.

Published by Elsevier Ltd.

1. Introduction

1.1. Background

In the past two decades observations of biological-based thin layers have become a common occurrence in the coastal ocean (Donaghay et al., 1992; Holliday et al., 1998). A variety of acoustic and optical sensors and specialty platforms have been developed to detect different types of thin layers. These include thin layers of: phytoplankton, zooplankton, marine snows, viruses and bacteria (Alldredge et al., 2002; McManus et al., 2003). In addition now emerging is the capability of obtaining simultaneous local measurements of the surrounding physical flow field. However, there have been very few direct and simultaneous biological and turbulence measurements within and surrounding the thin layers. Simultaneous fine and micro-scale physical and biological measurements are particularly important since ocean stratified turbulence typically occurs on the same vertical scale as that of thin layers, namely several meters to several centimeters.

Some limited observations of aspects of the turbulent field in the neighborhood of thin layers have been made. These typically either involve estimating the local Richardson number (Dekshenieks et al., 2001) or using temperature microstructure as a surrogate for the turbulent kinetic energy dissipation rate, ε (Alldredge et al., 2002; McManus et al., 2003). Both of these methods of inferring turbulence are indirect and subject to a number of assumptions which may not always be relevant to the local physical environment (Luketina and Imberger, 2001; Thorpe, 2005).

Turbulence is an ubiquitous feature in the ocean and is thought to have, at times, a significant effect on plankton evolution and behavior (Sullivan and Swift, 2003; Mann and Lazier, 2006). A number of physical mechanisms associated with turbulence have been postulated to have a critical role on a plankton community such as that occurring in a thin layer. These mechanisms include: mixing and stirring (Mann and Lazier, 2006), a balance between vertical straining and vertical diffusion (Stacey et al., 2007), and a change in predator–prey contact rate (Rothschild and Osborn, 1988). However, since, up until very recently, it has been very difficult to measure in situ both the local turbulent and plankton fields, the variety of different theories lack direct confirmation.

Laboratory experiments have often been used to try to understand the relationship of turbulence to organism behavior and response. Examples of such laboratory experiments include organism trajectory in a turbulent field (Kamykowshi, 1995); the effect of turbulence on diel vertical migration (Park et al., 2002); and the effect of turbulence on growth rate and mortality (Sullivan and Swift, 2003). Various researchers have examined the effect of turbulence on different species of phytoplankton, including diatoms and dinoflagellates, which are the major phytoplankton species observed in the LOCO field experiment in

* Corresponding author. Tel.: +1 508 910 6337; fax: +1 508 910 6376.
E-mail addresses: zwang@umassd.edu (Z. Wang), lgoodman@umassd.edu (L. Goodman).

0278-4343/$ - see front matter Published by Elsevier Ltd.
doi:10.1016/j.csr.2009.08.006

Monterey Bay, CA, the location of the data discussed in this manuscript. Both enhanced and suppressed growths have been observed in these experiments.

These studies suggest that turbulence has a variety of competing effects on planktonic organisms. It can change the size and growth rate of organisms, deliver or take away nutrients and wastes from organisms, and increase or decrease the encounter rate with nutrients and light. In addition the effects of turbulence intensity level may be organism specific. When a species is subject to an increase of turbulence shear, it may increase the uptake of one nutrient while decreasing the uptake of another. Critical to the effectiveness of these processes is whether the turbulence is sufficiently strong to embed the nutrients and phytoplankton into its flow field.

1.2. Recent field work

With the advent of modern physical and biological tools and techniques of observing fine and micro-scale phenomena, researchers are accelerating their field observations of the role of turbulence on thin layer generation, evolution, and decay. Recent observations by Dekshenieks et al. (2001), Alldredge et al. (2002), and McManus et al. (2003, 2005) have suggested that thin plankton layers only occur in an environment of relatively weak turbulence. However in these studies the occurrence and estimated level of turbulence is inferred either from an estimate of the local Richardson number (Dekshenieks et al., 2001) or from temperature microstructure measurements (Alldredge et al., 2002; McManus et al., 2003, 2005). A Richardson number criterion only insures instability at the local time and location of its occurrence when it is below some critical value, typically 0.25. It does not guarantee that turbulence will evolve nor does it yield information on the intensity, spatial structure, and duration of the turbulent field. Temperature microstructure is not necessarily directly related to velocity turbulence, which is a key physical quantity necessary to understand the dynamics of a turbulent field. In addition, because of the limited response time of the fastest available temperature sensors, and since temperature diffuses seven times slower than velocity, it may not be possible to resolve temperature variability to a sufficiently small scale to allow an estimate of thermal dissipation rate, χ, (Sherman and Davis, 1995), an essential quantity used to infer both the turbulent diffusivity, κ_ρ as well as the turbulent kinetic energy dissipation rate, ε.

The approach described in this manuscript is the usage of a specially equipped AUV, the T-REMUS, to obtain collocated and simultaneous velocity turbulence, velocity and density fine scale variability, and the chlorophyll *a* signature of a thin layer. In two recent manuscripts, Goodman and Wang (2009) and Wang and Goodman (2009), detail the approach and technique of using the AUV for simultaneous turbulence and thin layer measurements.

In this manuscript we will concentrate on the role of the turbulent eddy velocity and turbulent intensity on the evolution of the spatial structure of a thin layer. Particular attention will be given to developing criteria for conditions in which organisms will behave as passive Lagrangian tracers. We will examine in detail a data set which clearly shows the evolution of an initially strong compact spatially extensive thin layer being advected into the experimental site and then undergoing diffusion.

In Section 2, Approach, a brief summary of the T-REMUS and its sensor systems are described. More details can be found in Goodman and Wang (2009). In Section 3, Theoretical Background, we discuss the physical parameters which can be estimated from the in situ data and used in our subsequent analyses on thin layer evolution. We also develop parameters and criteria for when particles can be entrained in a turbulent field and behave as passive Lagrangian tracers. We use results from a model based on the homogenous and inhomogeneous damped harmonic oscillator equation. In Appendix A: Modeling Phytoplankton as a Stokes Particle in a Buoyancy Field, the mathematical details to this approach are given. In Section 4, A Case of Thin Layer Turbulent Dispersion, we present and discuss the case of a thin layer undergoing advection and turbulent diffusion. In Section 5 we apply the theories of Sections 3 and 4 to quantify the conditions under which the chlorophyll *a* thin layer field has remained compact and under which it disperses. Section 6 gives the Summary and Conclusions.

2. Approach

2.1. Platform and sensors

The platform used to collect data is the autonomous underwater vehicle, T-REMUS, which is an extended version of the Hydroid Inc. REMUS 100 vehicle. T-REMUS is 2 m long, has a diameter 0.2 m and weighs 63 kg in air. It is equipped with: a SBE 49 FASTCAT CTD; an upward and downward looking 1.2 MHz RDI ADCP; a Rockland Microstructure Measurement turbulence System (RMMS); and an ECO BB2F backscattering meter and chlorophyll fluorometer. It also contains a suite of hotel sensors to monitor the six degree of motion of the AUV. Tracking occurs using both a long and short baseline in water acoustic system. The T-REMUS was programmed to operate in a 5° yo-yo mode. It underwent a vertical excursion between 1 m depth from the surface to 4 m depth above the bottom. Horizontal ground speed was approximately constant at 1.2 m s^{-1}.

Turbulent velocity gradients are obtained from the two orthogonal thrust probes in the RMMS unit. The unit also contains a three vector component accelerometer, two fast response FP07 thermistors, and a fast response pressure sensor. A vehicle motion decontamination technique (Goodman et al., 2006) using this suite of supporting sensors is used to minimize spurious motion contamination on the turbulence sensors. The RMMS data is digitized and then stored at the rate of 500 Hz, the SBE 49 FASTCAT CTD at 16 Hz, and BB2F optical data at 1 Hz. The upward and downward 1.2 MHz Acoustic Doppler Current profiler contains 32 bins, each spaced 0.5 m apart. There is a 1.2 m blanking distance, centered both upward and downward about the vehicle. The WETLabs BB2F sensor measures chlorophyll *a* at 470 nm and scattering at 470 and 700 nm. Thin layers are identified principally using the chlorophyll *a* channel.

During the LOCO 2006 field effort, shown in Fig. 1a, a bottom-mounted upward-looking 1.2 MHz ADCP (courtesy of Stacey) and an accompanying thermistor chain (courtesy of Holliday) were deployed near the T-REMUS survey area at a fixed mooring station, labeled "K1" in Fig. 1b. The ADCP velocity data was averaged over 5 min. The chain contained 15 thermistors, with a vertical separation of 1 m except near the surface and bottom, where the separation distance was 2 m. The sampling rate for this data was 1/30 Hz.

2.2. Experimental site

Monterey Bay (MB) is a semi-enclosed bay located between 36.55 and 37.00°N off the west coast of United States (Fig. 1a). It has an open connection to the ocean and has very limited fresh water input. The color map in Fig. 1a shows the topography in Monterey Bay. Along with its deepness and broadness, Monterey Bay is not an estuary as it is not significantly diluted by the fresh

Please cite this article as: Wang, Z., Goodman, L., The evolution of a thin phytoplankton layer in strong turbulence. Continental Shelf Research (2009), doi:10.1016/j.csr.2009.08.006

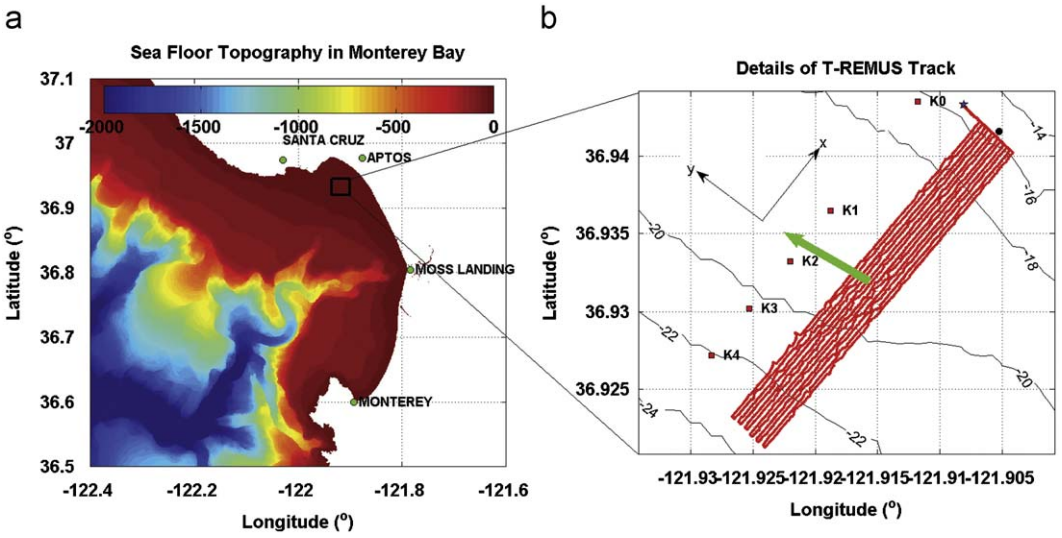

Fig. 1. (a) Sea floor topography in Monterey Bay, CA, USA. The horizontal scale is water depth (m). The site of LOCO 2006 experiments is denoted by the black rectangle. (b) Details of T-REMUS track (red lines) in the northern bight of Monterey Bay, CA on 24 July 2006. There are twelve parallel lines, each of an across isobath distance of ~2.5 km. Black contour lines are water depth in meters. The green arrow indicates the direction of the vertically averaged current on 24 July 2006. The black filled circle is the reference point used to calculate the AUV offshore distance. K1 is a fixed mooring station deployed by other LOCO groups. (For interpretation of the references to colour in this figure legend, the reader is referred to the web version of this article.)

water influx except temporally during brief periods of large river discharge (Breaker and Broenkow, 1994). The effect of terrestrial input can be ignored due to the small precipitation during LOCO 06. The Bay is symmetrical in shape and divided approximately equally into a northern and southern sector by the Monterey Submarine Canyon (MSC). The MSC, is the major topographic feature in MB, and has a very important role in transporting nutrients from the deep ocean to the shallower coastal regions by the internal tide (Shea and Broenkow, 1982). Although MSC represents a major depression of the bay, a major fraction of the bay is very shallow. Approximately 80% of the Bay, 440 km^2, is shallower than 100 m and only 5% is deeper than 400 m (Breaker and Broenkow, 1994). There are two bights in MB, one to the south near Monterey and a second to the north between Santa Cruz and Aptos. The LOCO 06 T-REMUS experiment took place in the northern bight of Monterey Bay. The average water depth in the experimental area is 19 m, with the bottom depth ranging from 16 to 23 m (Fig. 1b). The red parallel lines in Fig. 1b show the detailed track of T-REMUS AUV during LOCO 2006 experiment. The vehicle was deployed and recovered at the same location as shown by the blue star in Fig. 1b. The AUV performed a series of 12 across isobath tracks over an eight hour period. These tracks were approximately perpendicular to isobath contours. Each track consisted of approximately 15 profiles with the horizontal distance between profiles being on average 150 m apart. The green arrow shows the direction of the mean current field, which is principally along the direction of the mean isobath for the time period of the T-REMUS 24 July 2006 experiment. Its magnitude is approximately 0.15 m s^{-1} from measurements of the T-REMUS based ADCP.

3. Theoretical background

Two fundamental fine scale and micro-scale physical parameters of direct relevance to turbulence in a stratified fluid can be estimated from the suite of sensors on the T-REMUS. These are: (1) the local buoyancy frequency, N, (resolution of order 0.1 m vertically) which is obtained from the yo-yoing FASTCAT CTD, and (2) the turbulent kinetic energy dissipation rate, ε, (resolution of order 0.5 m vertically) obtained from the RMMS system. (See MacDonald et al., 2007 for a description of the technique of estimating the TKE dissipation rate.) With these two parameters we can derive three turbulence parameters of direct relevance to thin layer evolution. These are: (i) the buoyancy Reynolds number, Re_b; (ii) the turbulent eddy diffusivity, κ_ρ; and (iii) the turbulent eddy velocity, w_e. Note that of the three turbulent quantities only two are independent, since they are all functions of the two independently measured quantities, ε and N.

The buoyancy Reynolds number is defined by

$$\mathrm{Re}_b = \frac{\varepsilon}{\nu N^2} = \left(\frac{l_B}{l_\nu}\right)^{4/3} \tag{1}$$

where we have written the right hand side of Eq. (1) in terms of the ratio of the buoyancy or Ozmidov scale $l_B = (\varepsilon/N^3)^{1/2}$ to the Kolmogorov length scale $l_\nu = (\varepsilon/\nu^3)^{-1/4}$, that is the ratio of the largest scale expected to be present in a turbulent velocity field in a stratified turbulent environment, l_B, to the smallest scale, l_ν (Tennekes and Lumley, 1972). The subscript $\nu \approx 10^{-6}$ m^2 s^{-1} refers to the molecular kinematic viscosity of seawater. The buoyancy Reynolds number, Re_b, is an indicator of the spatial dynamic range of the turbulent field. As turbulent intensity increases, Re_b increases. Laboratory and field observations (Istweire et al., 1993; Sander et al., 2000) have indicated that for $\mathrm{Re}_b < 20$ turbulence ceases to exist because of the intense influence of the local stratification. For $\mathrm{Re}_b < 200$ turbulence is anisotropic even at the smallest scales (Yamazaki and Osborn, 1990; Gargett et al., 1984). That is when the ratio of the largest to smallest scales, (l_B/l_ν), is less than that of order $(200)^{3/4} \approx 53$ turbulence in the vertical direction is suppressed relative to the horizontal directions. It is straightforward using Eq. (1) and the concept of a mixing efficiency $\Gamma \equiv (B/\varepsilon)$, where B represents the rate of change of potential energy due to turbulent mixing, to relate the eddy diffusivity $\kappa_\rho \equiv (\langle \rho' w' \rangle / (\partial \overline{\rho}/\partial z))$ to Re_b (Goodman and Wang, 2009), whence it follows that

$$\kappa_\rho = \frac{\langle \rho' w' \rangle}{(\partial \overline{\rho}/\partial z)} = \frac{\Gamma \varepsilon}{N^2} = \Gamma \nu \mathrm{Re}_b \tag{2}$$

Typically $\Gamma \approx 0.2$ is assumed (Osborn, 1980; Gregg, 1987).

Using Eq. (2) with $\Gamma \approx 0.2$ the boundary limits of no turbulence, $\mathrm{Re}_b = 20$, and that of anisotropic small scale turbulence

Please cite this article as: Wang, Z., Goodman, L., The evolution of a thin phytoplankton layer in strong turbulence. Continental Shelf Research (2009), doi:10.1016/j.csr.2009.08.006

$Re_b = 200$, correspond to eddy diffusivities of $\kappa_\rho = 4\times10^{-6}\,m^2\,s^{-1}$, and $\kappa_\rho = 4\times10^{-5}\,m^2\,s^{-1}$ respectively. We will thus use the terminology of weak turbulence to refer to turbulence characterized by $Re_b<200$ and strong turbulence when $Re_b\geq200$. As discussed in Goodman and Wang (2009) and also shown in the present study, there are cases of relatively large dissipation rates at the T-REMUS LOCO site, characterized by $\varepsilon>10^{-8}\,m^2\,s^{-3}$, but associated with marginally active turbulent patches where $Re_b\approx200$. We see also from the relationship given by Eq. (2) that for such weak turbulence the eddy diffusivity is only a factor of 4 larger than the molecular kinematic viscosity. Thus the dissipation rate alone is not a sufficient measure to indicate the intensity of the turbulent field or its effectiveness in diffusing an embedded scalar such as a phytoplankton field. This is very important in analyzing the impact of turbulence on the potential of weakening a thin layer by turbulent diffusion.

Finally we need to determine if the phytoplankton will become embedded in the turbulent field. We will now show that this is determined by ratio $r=(w_{rel}/w_e)$, where w_{rel} is the speed of plankton relative to that of the turbulent field from either buoyancy control, sinking, or self-propulsion (swimming); w_e is a typical speed of the energetic turbulent eddies.

Consider first the case of non-swimming phytoplankton whose motility is produced by buoyancy changes. Following the approach of Stacey et al. (2007) we model the forcing on such an organism due to buoyancy as $F_{\boldsymbol{B}} = -\Delta\rho gV = \rho VN^2z$ where ρ is the fluid density, $\Delta\rho$, the density difference between the particle and the surrounding fluid, N, the local buoyancy frequency, V the particle volume, g the gravitational acceleration and, z, the vertical (across isopycnal) displacement of the fluid from its equilibrium position. Stacey et al. (2007) consider the phytoplankton like particle as spherical. Because of the very low Reynolds number, $R=(w_{rel}L/\nu)$ of order 1 or less expected for the case of non-swimming phytoplankton, this type of model can be generalized by either considering particles whose vertical and horizontal dimensions are different, such as oblate spheroids, or, in the extreme case, as long cylinders oriented perpendicular to the flow. In the above expression for R, w_{rel} is a characteristic particle velocity relative to the fluid, L its characteristic length in the direction of flow, and ν molecular kinematic viscosity. For the former case provided, the ratio of the major to minor axis is of order 1 the diameter to be used in the Stokes flow would be replaced by some equivalent diameter, $D_{\text{equivalent}}$, defined by $V=(1/6)\pi(D_{\text{equivalent}})^3$. In Appendix A "Modeling Phytoplankton as a Stokes Particle in a Buoyancy Field" we model the vertical equation of motion of a Stokes particle as a damped harmonic oscillator. We present results for the two end point cases, the sphere, and the long cylinder. For both cases, provided the particle Reynolds number $R=(w_{rel}L/\nu)$, is of order 1 or less, in the absence of external forcing the particle motion can be approximated by the unforced damped harmonic oscillator equation, Eq. (A-3), namely

$$\frac{d^2z}{dt^2}+\frac{1}{\tau}\frac{dz}{dt}+AN^2z=0 \tag{3}$$

In Eq. (3) to generalize beyond the spherical particle model of Stacey et al. (2007), we will take A of order 1 noting that $A=(2/3)$ for a spherical particle and $A=(1/2)$ for the cylindrical case, the two limiting cases of particle shape. In Eq. (3) τ is the response time due to the Stokes drag. When Reynolds number R is of order 1 or less $\tau=\tau_s=(D^2/12\nu)$ and $\tau=\tau_c=(D^2/4\nu)$ for the case of the sphere and long cylinder, respectively. (See Appendix A and Batchelor, 1994.) D is the particle diameter (either sphere or cylinder) and ν the kinematic viscosity of the surrounding fluid. In general the type of diatoms present at the LOCO site (see Rines et al. this issue) are much more complicated than either a pure spherical shape or cylindrical shape, sometimes being a long chain of individual diatoms. Nonetheless for R of order 1 or less which is the regime in which the Stokes drag law is valid, for a particle in a stratified fluid we expect Eq. (3) to remain approximately valid, with τ of the form

$$\tau = C\frac{D^2}{\nu} \tag{4}$$

where $(1/12)<C<(1/4)$. This is expected since when R of order 1 the drag force is linearly proportional to the ratio of the particle volume to its wetted surface area. The sphere and infinite cylinder represent the two end points for that ratio. Using a similar argument we would expect A in Eq. (3) also to be of order 1 since A depends on the ratio of the particle volume to the particle volume plus the "added" volume by inertia effects (Newman, 1977). In the Appendix A we find the solution to Eq. (3) for a particle being initially displaced l from its equilibrium position. For the expected case of

$$N\tau \ll 1 \tag{5}$$

the particle is highly damped and can be shown to have a maximum velocity, $w_p = w_{rel}$, given by

$$w_{rel} = AlN^2\tau \approx lN^2\tau \tag{6}$$

where we have taken $A\approx1$. Again we have used the subscript notation "*rel*" to indicate that the velocity is calculated relative to the fluid, which in this case is $w_e=0$. Turbulent forcing adds a term of the form $f=f_T=(w_e/\tau)+AN^2z_T$ on the right hand side (RHS) of Eq. (3) resulting in the inhomogeneous damped harmonic oscillator Eq. (A-14).

Let us examine the nature of the turbulent forcing. Since we expect that the maximum turbulent displacement to be of order the Ozmidov (buoyancy) scale, $z_T\sim l_B$ and the turbulent eddy velocity given by $w_e\approx Nl_B$ (Tennekes and Lumley, 1972) then if $N\tau\ll1$, $f_T\approx(w_e/\tau)$ and using the forced solution (A-16) and assuming that the characteristic time scale of the turbulent forcing is N^{-1} it is straightforward to show that the particle velocity is given by $w_p=w_e+O(N\tau)$. This result can also be obtained by substituting $w_e\approx Nl_B$ in Eq. (6), resulting in $w_{rel}=w_p-w_e=N\tau w_e$ and thus

$$\left|\frac{w_{rel}}{w_e}\right| = N\tau \ll 1 \tag{7}$$

Eq. (7) is a restriction on the size of particles arising from the condition of $N\tau\ll1$. For the case of swimming (self propelled) plankton, we can employ the same approach used in modeling the propulsive force of a self propelled underwater vehicle maintaining some speed w_p (Nahon, 1996). In this case we would add to the turbulent forcing the propulsion term, f_p, given by $f_p=(w_p/\tau)$ to the RHS of Eq. (3), with $F_p=(\rho(V+V_{\text{added}})w_{rel})/\tau$ the propulsive force in overcoming the Stokes drag in a fluid moving with speed w_e. The turbulent forcing term $f_T=w_e/\tau$ will then dominate the particle self propulsive forcing term provided

$$\left|\frac{w_{rel}}{w_e}\right| \ll 1 \tag{8}$$

is satisfied and the Reynolds number is of order 1. (Note for Reynolds number $R\gg1$ the propulsive force would satisfy a quadratic drag law with the constraint on the square of the ratio $|w_{rel}/w_e|$ given by $|w_{rel}/w_e|^2\ll1$, a much less restrictive criterion than Eq. (8).) For the cases of a phytoplankton using buoyancy control and/or self-propulsion, with R of order 1, Eq. (8) is then the criterion to determine if it will become embedded in a turbulent field and then subsequently act as a passive Lagrangian tracer. For a non-swimming buoyancy controlling organism Eq. (5) can be used for that criterion.

To estimate w_e, we follow the physical scaling arguments of Tennekes and Lumley (1972) whence the velocity of the most

Please cite this article as: Wang, Z., Goodman, L., The evolution of a thin phytoplankton layer in strong turbulence. Continental Shelf Research (2009), doi:10.1016/j.csr.2009.08.006

energetic turbulent eddies in a stratified fluid would be given by

$$w_e = a\sqrt{\frac{\varepsilon}{N}} \tag{9}$$

where a is some dimensional constant of order 1. We will take $w_e = \sqrt{\varepsilon/N}$ to represent a typical value of the root mean square (rms) turbulent eddy velocity. As such w_e in Eq. (9) with $a = 1$ will be used in identifying environments which satisfy the criteria of Eq. (8), which is insensitive to the numerical constant a in Eq. (9) provided it is of order 1.

4. A case of thin layer turbulent dispersion

In this section we will examine the spatial evolution of a thin layer observed in the 24 July 2006 T-REMUS experiment. In Fig. 2, we show time series contour maps of across and along isobath velocity (Figs. 2a and b) and of isotherm displacement (Fig. 2c) for the time period of 12:00 h 24 July–06:00 h PDT (Pacific Daylight Time) 25 July 2006 at the K1 site. These are obtained, respectively, from the bottom-mounted upward-looking 1.2 MHz ADCP and the moored thermistor chain. Positive across isobath currents are onshore, positive along shore currents are to the northwest. The K1 site is +400 m perpendicular in the along isobath direction to the T-REMUS tracks. See Fig. 1b. The two thick vertical lines on the three contour maps of Fig. 2 indicate the time period of the T-REMUS deployment, namely from 17:00 h 24 July to 01:00 h PDT 25 July 2006. Note the strong diurnal cycle in velocity. The tides in Monterey Bay are mixed, with K1, O1, M2 and S2 constituents contributing approximately 80% of the tidal variation (Breaker and Broenkow, 1994). At this site, during this period of time, the velocity data suggest that diurnal tides dominate. As expected, the along isobath velocity is larger than the across isobath velocity with the former reaching maximum values of order 0.15 m s^{-1} while the latter at times do reach a maximum value of order 0.1 m s^{-1}. The mean flow during the T-REMUS deployment is to the northwest, as indicated in Fig. 1b from the T-REMUS ADCP averaged vector current estimate, in approximate agreement with the fixed station data of Figs. 2a and b. It should be noted that for the time period of the 24 July the T-REMUS deployment, which started at 17:00 PDT, the tides changed from flood to ebb.

The isotherm contours of Fig. 2c clearly indicate the appearance of internal solitary waves during the 24 July 2006 T-REMUS deployment. Internal waves associated with the baroclinic tide are expected to occur in Monterey Bay, where it has been hypothesized that the strong topographic features present in Monterey Bay, such as at the edge of the Monterey Bay Canyon, are near ideal sources of generation of the internal tide and associated internal solitary waves (Baines, 1986; Kunze et al., 2002; Carter et al., 2005). Note that at 17:00 PDT, the time of the beginning of

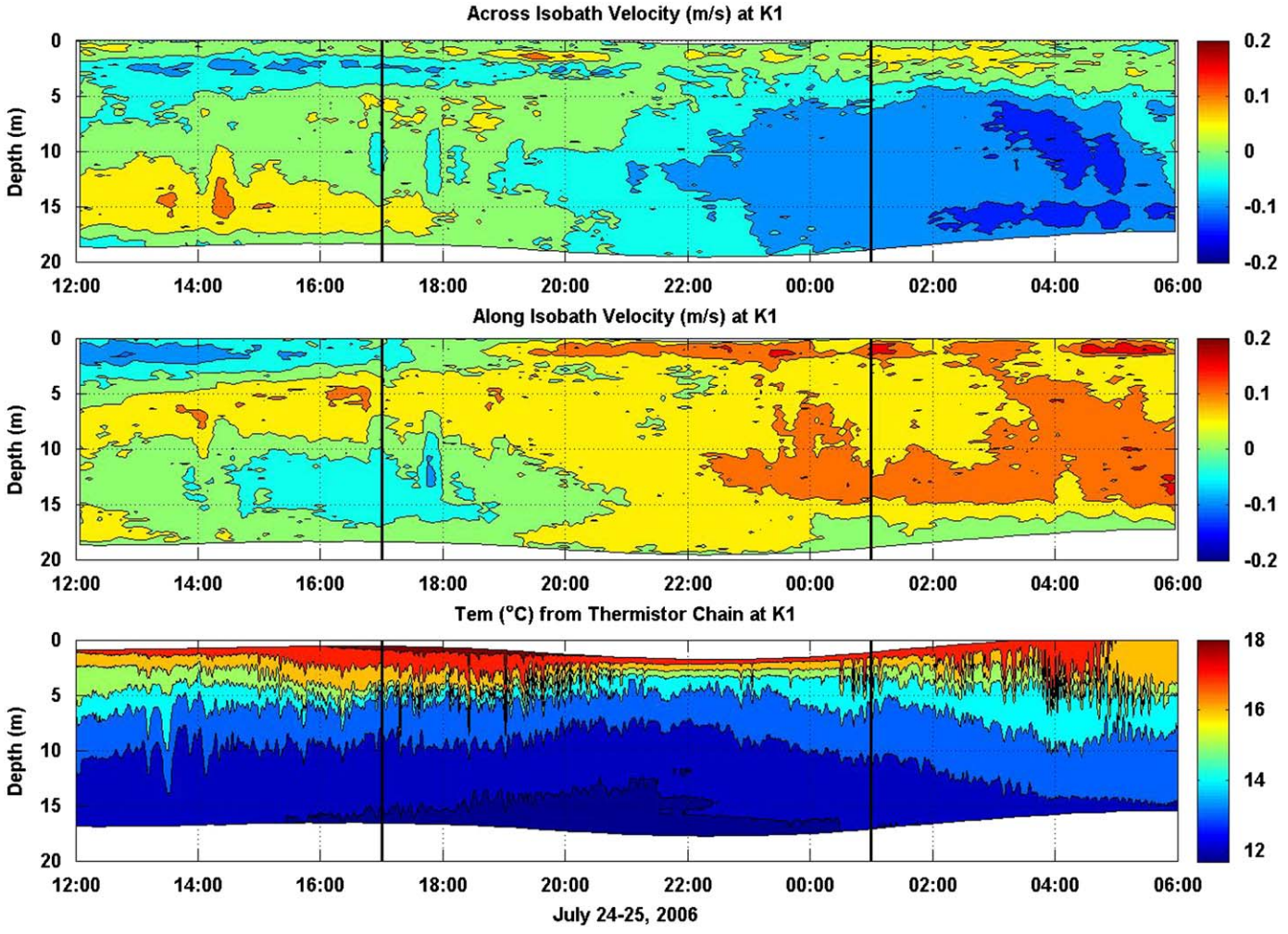

Fig. 2. Contour maps at K1 fixed station the time period of 12:00 h 24 July–06:00 h Pacific Daylight Time (PDT) 25 July 2006. (a) Across isobath velocity; (b) along isobath velocity and (c) temperature from thermistor chain. The current in (a) and (b) are measured from bottom-mounted ADCP. The data between the two vertical black lines show the time period of the T-REMUS experiment between 17:00 h, 24 July 2006 and 01:00 h PDT, 25 July 2006.

Please cite this article as: Wang, Z., Goodman, L., The evolution of a thin phytoplankton layer in strong turbulence. Continental Shelf Research (2009), doi:10.1016/j.csr.2009.08.006

the 24 July 2006 T-REMUS deployment, there is already an internal wave train present at the experimental site. By 20:00 PDT this internal wave train has propagated out of the experimental site although at the very end of the experiment a new wave train begins to occur.

For indicating a thin layer, we use the chlorophyll *a* signature obtained from our T-REMUS mounted WETLabs BB2F sensor package. For details on the types of organisms present at the LOCO site during this time period and their resulting chlorophyll *a* signature, see the article of Rines et al. in this special issue.

4.1. Definition of chlorophyll a thin layers

The key issues in defining a thin layer are to determine some minimal magnitude and a criterion for upper and lower boundaries. To this end we combine the criteria developed by Dekshenieks et al. (2001) and Sullivan et al. (this issue), namely:

(i) The maximum chlorophyll *a* value in the layer must exceed that of three times of background levels.
(ii) The thin layer must contain at least three data points.
(iii) The full-width-half-maximum (FWHM) vertical thickness of the thin layer must be less than 3 m.
(iv) The thin layer feature must be present in 2 or more subsequent profiles.
(v) The absolute value of the chlorophyll *a* gradient at the upper and lower boundaries must exceed a certain critical value.

The background value used is taken in the region below which the thin layers occurred, namely at depths where the temperatures was less than $T = 14\,^{\circ}\mathrm{C}$. This leads to a background concentration of $c_{bg} = 2.6\,\mu g/l$ and the concentrations in the thin chlorophyll *a* layer must be three times greater than that value. The gradient criterion (v) for a thin layer is taken as $2\,\mu g\,l^{-1}\,m^{-1}$.

4.2. Spatial structure

In Figs. 3–6 from the T-REMUS observations, we show as a function of across isobath distance and depth, contour plots of temperature (°C), chlorophyll *a* ($\mu g\,l^{-1}$), the TKE dissipation rate, ε ($W\,kg^{-1}$) and the turbulent eddy diffusivity, κ_ρ ($m^2\,s^{-1}$). In Figs. 5 and 6 note that $\log_{10}$ of ε and κ_ρ are plotted. The across isobath distance is referenced to the initial T-REMUS position at 36.94°N, 121.91°W, which is shown as the black filled circle in Fig. 1b. Note that there are 11 contour maps in Figs. 3–6, extending over an 8 h period. The 7th track leg space is left blank as, during this time period, the vehicle was programmed to run at a constant depth for calibration. The average location of the AUV derived yo-yo data profiles, used to make the contour plots, are shown on the top of each panels, and numbered in the order of collection. Each profile

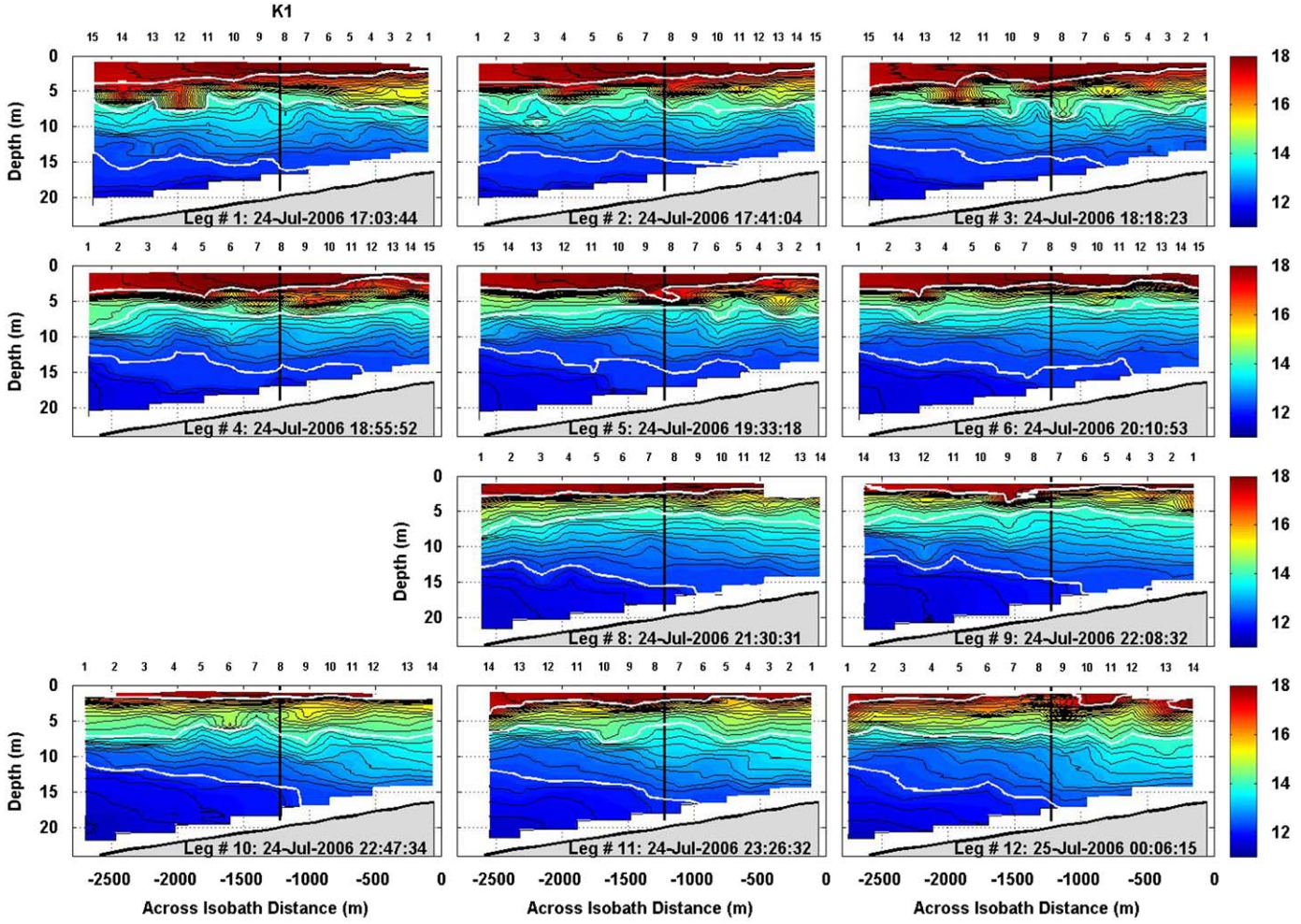

Fig. 3. Contour maps of the temperature (°C) field as a function of across isobath distance and depth in 24 July 2006 experiment. Isotherms of temperature spaced 0.2 °C apart are shown as black contour lines except isotherms of $T = 12.2$, 14 and 17.4 °C, which are emboldened in white. The vertical thick black line shows the along isobath location of station K1.

Please cite this article as: Wang, Z., Goodman, L., The evolution of a thin phytoplankton layer in strong turbulence. Continental Shelf Research (2009), doi:10.1016/j.csr.2009.08.006

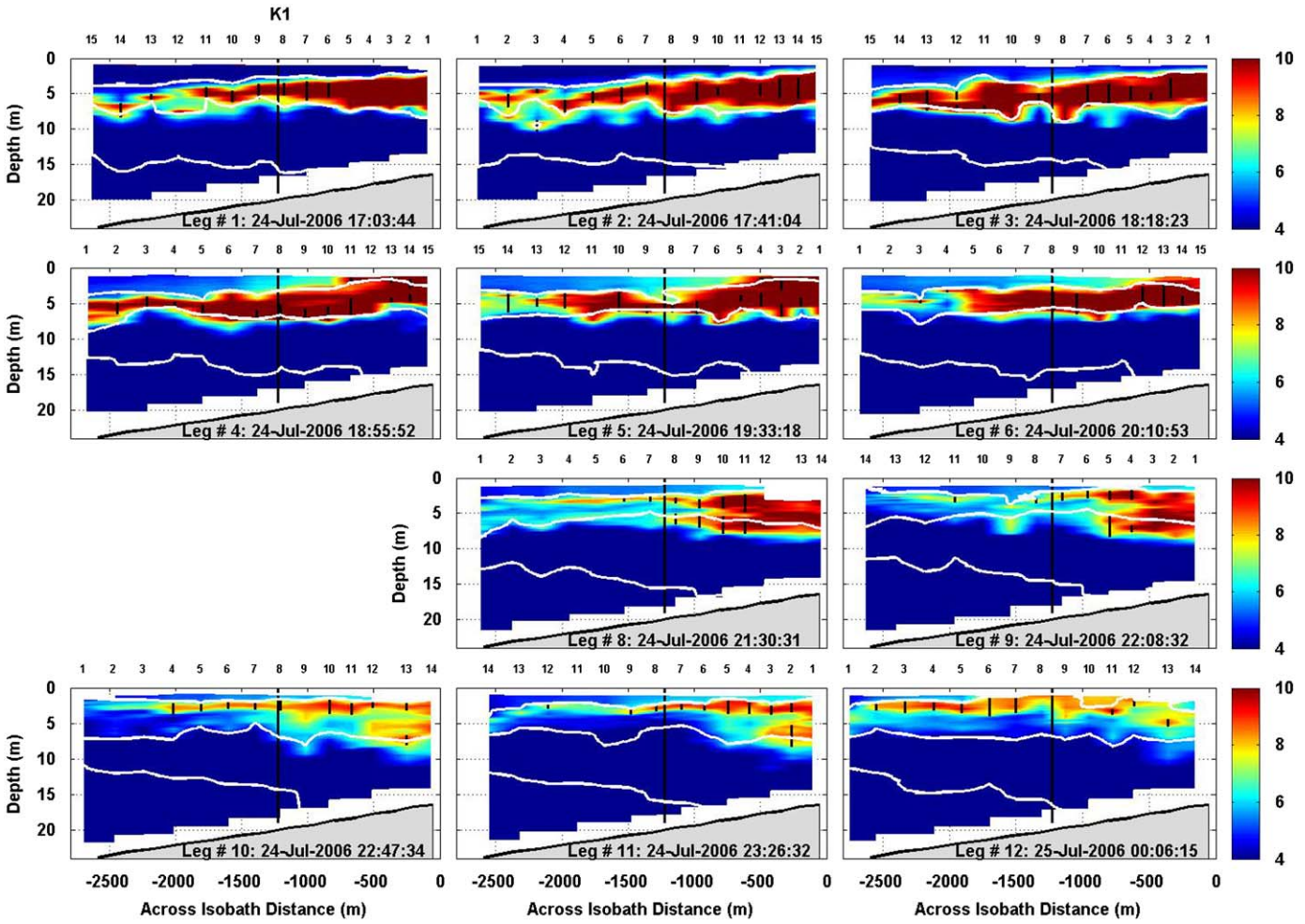

Fig. 4. Contour maps of the chlorophyll *a* ($\mu g\,l^{-1}$) as a function of across isobath distance and depth in 24 July 2006 experiment. Isotherms of $T = 12.2$, 14 and 17.4 °C are emboldened in white. Thin chlorophyll *a* layer is indicated at each profile location by a superimposed solid black vertical line.

on average was separated approximately 150 m horizontally. The dark black line above the gray area indicates the bottom, which ranged from 16 to 23 m. The vertical thick line is the along isobath location of the K1 station, which is the location of the data shown in Fig. 1b.

During the period of T-REMUS 06 LOCO experiment, salinity changes are very small and isotherms are a good surrogate for isopycnals (Wang and Goodman, 2009). In each of these contour plots, isotherms are displayed as black lines with the exception of three isotherms which indicate boundaries. These are the isotherms of $T = 12.2$, $T = 14$ and $T = 17.4$ °C. These isotherms are indicated by the thick white contour lines and separate four different layers: (1) the surface layer; (2) an upper thermocline; (3) a lower weaker thermocline; and (4) the bottom layer. Note the change in the location of the foot of the bottom water from the motion of the $T = 12.2$ °C boundary isotherm in subsequent panels. During the first half of the experiment movement of this isotherm indicates an upslope movement of bottom water. This same feature was noted in the 17 July 2006 LOCO data by Goodman and Wang (2009) and most probably is associated with the baroclinic internal tide.

From Fig. 3, the surface layer is easily seen by the appearance of warm water, indicated by the red color in each of the panels. At the beginning of the experiment it is approximately 8 m in thickness at the offshore end and somewhat thinner, onshore, ~5 m, and somewhat warmer there. Note that the upper layer depth decreases with time and by the end of the experiment becomes less than 2 m. This feature is consistent with the temperature chain measurements shown in Fig. 2c, which indicate the warm near surface water shoaling with time, starting at approximately 20:00 PDT, 24 July 2006, a time close to sunset.

The upper thermocline, located between the $T = 14$ and 17.4 °C isotherms, is characterized by very strong stratification, having a vertical temperature gradient typically of order $\partial T/\partial z = 1.0\,°C\,m^{-1}$. In the lower thermocline stratification is weaker with a typical gradient of $\partial T/\partial z = 0.25\,°C\,m^{-1}$. During the first half of the experiment a number of large abrupt changes in isotherm depth are noted in the thermocline regions. This occurs during the same period of time when internal solitary waves were observed in the thermistor chain data at K1, Fig. 2c. Because the average distance between profiles used to estimate the AUV derived isotherms is of order 150 m, we expect that our sampling will result in a spatially aliased sampling of the internal solitary waves expected at this experimental site. Using the average buoyancy frequency from the observed site into the eKdv theory analysis of Goodman and Wang (2009) we estimate an internal solitary wave phase velocity of $0.15\,m\,s^{-1}$. From Fig. 2c we see internal solitary waves of temporal extent as short as 5 min which would result in a solitary length scale of order 45 m. The abrupt irregular changes in the isotherm boundaries (white lines) of Figs. 3–6 are indication of aliased spatial sampling. In the second half of the experiment after 21:30 PDT, starting with panel #8, isotherm vertical displacement as a function of across isobath distance is relatively smooth, in agreement with the character of isotherm displacement found at

Please cite this article as: Wang, Z., Goodman, L., The evolution of a thin phytoplankton layer in strong turbulence. Continental Shelf Research (2009), doi:10.1016/j.csr.2009.08.006

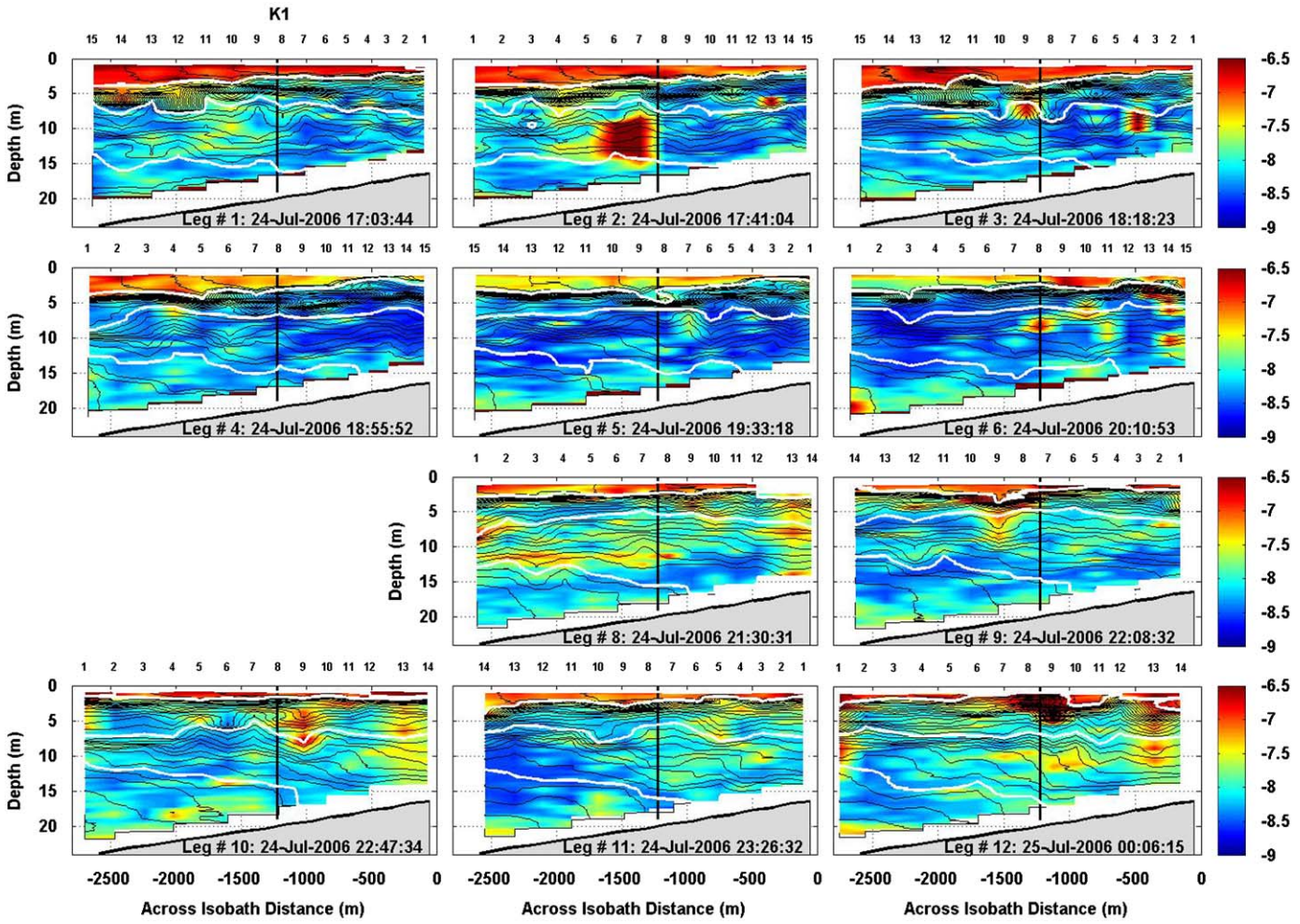

Fig. 5. Contour maps of the TKE dissipation rate, $\log_{10}(\varepsilon)$ W kg^{-1}, as a function of across isobath distance and depth in 24 July 2006 experiment. Isotherms identified in the same way as that shown in Fig. 3.

the fixed station K1 during this time period and characterized by the much weaker internal wave activity in the experimental site.

In Fig. 4, we show as a function of depth and across isobath location contour maps of chlorophyll *a* obtained from the AUV based BB2F fluorometer. The color bar scale to the right of figure is in units of $\mu g\,l^{-1}$. Using the criteria of a thin layer defined at the beginning of this section, a thin chlorophyll *a* layer (indicated at each profile location by a superimposed solid black vertical line) is noted in the upper thermocline throughout the experiment. In the first four panels, which cover a three hour period, the thin layer can be seen throughout the experimental region, with the largest chlorophyll *a* density occurring onshore of K1. The thin layer during this time period has a horizontal extent of order at least 2.5 km and may, in fact extend further onshore beyond the experimental area. Starting at 19:33 PDT, panel #5, the most offshore part of the thin layer starts to diminish, a process which continues throughout the remaining time of the experiment. Eventually the layer weakens and by the end of the experiment appears to be confined to a narrow depth range centered at a depth of 3.0 m. In panels #2 through 5, as noted previously, there is internal wave like vertical displacement of the isotherms and of the thin layer. Note, however that the thin layer, although displaced and distorted by this internal wave activity, remains intact with no indication of weakening through (turbulent) dispersion.

In Figs. 5 and 6, we present turbulent kinetic energy (TKE) dissipation rate and eddy diffusivity, plotted as $\log_{10}(\varepsilon)$ and $\log_{10}(\kappa_\rho)$, respectively. As shown in Eq. (2) the eddy diffusivity κ_ρ is linearly proportional to Re_b which, using a mixing efficiency of $\Gamma = 0.2$, results in the criteria of $\kappa_\rho > 4\times10^{-5}\,m^2\,s^{-1}$ (i.e. $Re_b \geq 200$) for strong turbulence. Note that the diffusivity, κ_ρ, contours of Fig. 6 highlight very different regions of turbulence than that of the TKE dissipation rate, ε contours in Fig. 5. The relative importance of turbulent mixing in the bottom mixed layer and, at times, in the thermocline, is clearly revealed in the κ_ρ contour plots but often not in the ε contour plots.

The most significant feature in the κ_ρ contour plots is that strong turbulence occurs predominantly in the surface and bottom layers. Near surface turbulence is most intense in the first two hours and characterized by $\kappa_\rho > 10^{-4}\,m^2\,s^{-1}$. It weakens with time and becomes shallower, being embedded in a shoaling upper ocean mixed layer. Turbulence in both upper and lower thermocline regions tends to be intermittent with most regions having weak turbulence characterized by $\varepsilon < 10^{-8}\,W\,kg^{-1}$ and $\kappa_\rho < 4\times10^{-5}\,m^2\,s^{-1}$. In panels #2, 3, and 4 of Fig. 6, which occur during the time period of the most intense internal solitary wave activity, there are regions of strong turbulence in the lower thermocline, closest to the bottom but few regions of strong turbulence in the upper thermocline. Turbulence occurring in the lower thermocline is predicted by theoretical work of Bogucki et al. (1997) and is most probably due to enhanced near bottom internal wave induced shear. Note the feature of strong isolated turbulence in panel #3 at $x = -1350$ m, near K1, occurring in what appears to be the lee of an isolated internal solitary wave. This feature is very similar to the features observed by Goodman and

Please cite this article as: Wang, Z., Goodman, L., The evolution of a thin phytoplankton layer in strong turbulence. Continental Shelf Research (2009), doi:10.1016/j.csr.2009.08.006

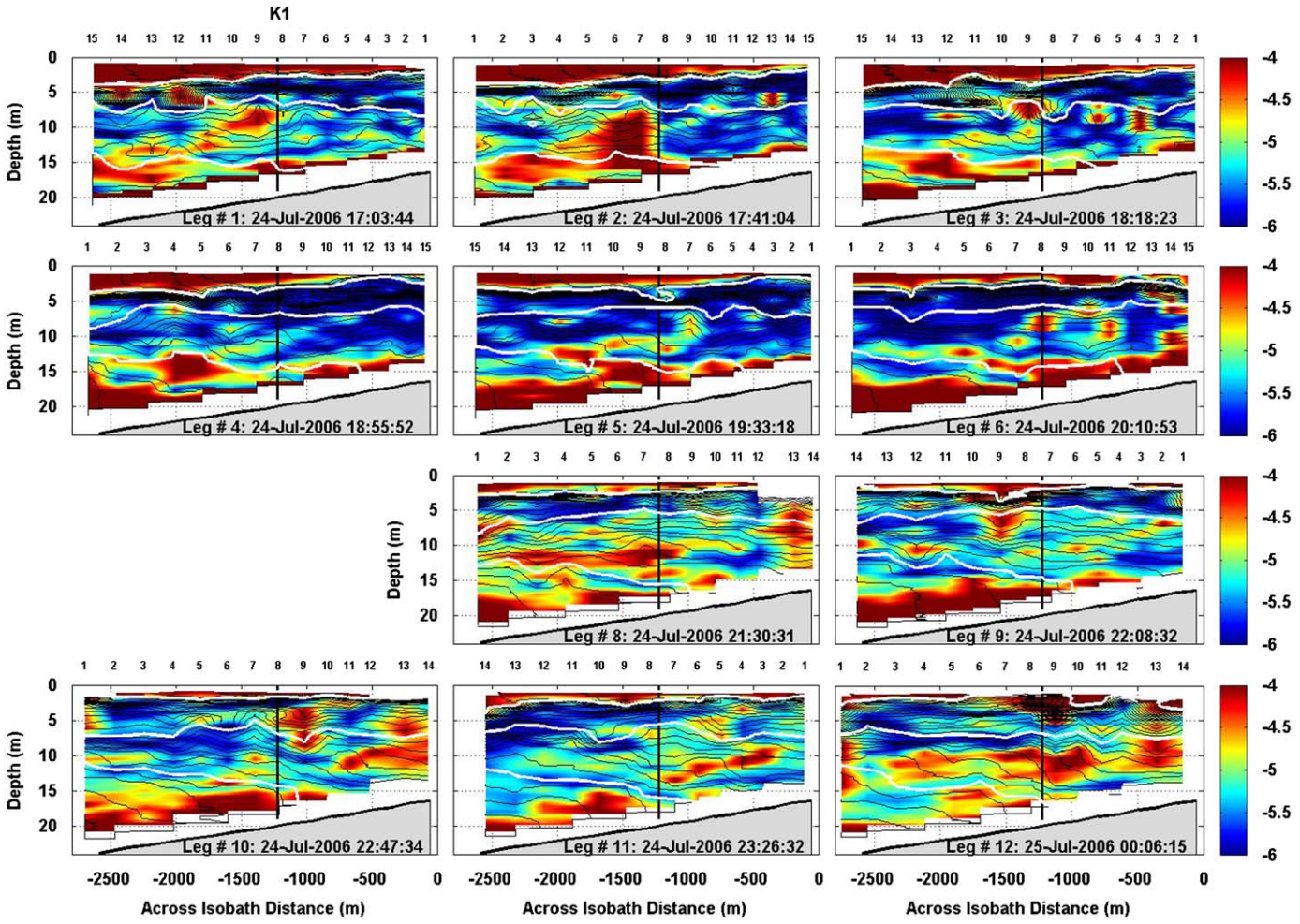

Fig. 6. Contour maps of the turbulent eddy diffusivity, $\log_{10}(\kappa_\rho)$ $m^2 s^{-1}$, as a function of across isobath distance and depth in 24 July 2006 experiment. Isotherms identified in the same way as that shown in Fig. 3.

Wang (2009) and Moum et al. (2003). The generation mechanism of this turbulence has been shown to be related to the vertical straining of the internal wave field on the background current field (Moum et al., 2003). This same mechanism was shown by Goodman and Wang (2009) to be responsible for turbulence generated in the wake of an internal wave train. However in this data set its occurrence is isolated resulting in a very limited spatial extent of the turbulent field.

During the second half of the experiment, particularly in panels #8 and 12 large horizontal across isobath regions of strong turbulence become present at the experimental site. By the end of the experiment, as shown in panel #12, strong turbulence appears in both the lower and upper thermocline depths throughout the observational area with the most intense turbulence increasing shoreward. In panels #8, 10 and 12, we see in the most shoreward location the entire water column undergoing strong turbulent mixing. We also see in panels #8, 10, and 12 of Fig. 4, chlorophyll *a* undergoing what appears to be a vertical diffusion at the most shoreward location.

5. Discussion

In this section we will apply the theoretical analyses given in Section 3 to the example thin layer evolution presented in Section 4. To that end we replot in Fig. 7 the κ_ρ contour plots shown in Fig. 6, but using temperature in place of depth as the ordinate. The dark black lines in Fig. 7 outline the boundary of the thin layer. We have used the criteria for the occurrence of a thin layer set forth in Section 4. This leads to the thin layer concentration, c, required to satisfy $c > 3 \times c_{bg} = 3 \times 2.6\,\mu g\,l^{-1} = 7.8\,\mu g\,l^{-1}$. The approach of using temperature (effectively density) as the ordinate minimizes the distortion effect of internal waves on the boundaries of the thin layer. The panels in Fig. 7 clearly show that the thin chlorophyll *a* layer occur in the upper thermocline between $T = 14$ and 17.4 °C.

The thin layer extends over the entire across isobath experimental range of 2.5 km in the first half (4 h), during which time period turbulent mixing within the thin layer is very weak, with $\kappa_\rho \sim 10^{-6}\,m^2\,s^{-1}$. Strong turbulence $Re_b \geq 200$ and $\kappa_\rho \gtrsim 4 \times 10^{-5}\,m^2\,s^{-1}$ within the thin layer only begins to occur in panel #6 and at the most seaward end of observations. During the second half of the experiment the thin layer has changed considerably. The most seaward part of the thin layer has decreased in vertical extent and weakened. However, unlike the 17 July 2006 data (Wang and Goodman, 2009) the turbulent field and the thin layer are not coincident. We see a number of patches of strong turbulence within the thin layer during this time period, with most such regions occurring in the most shoreward locations.

In Section 3 we have shown that a critical turbulent quantity affecting the evolution of a thin phytoplankton layer is the turbulent eddy velocity, w_e and the magnitude of the motility speed of the organism relative to the turbulence, w_{rel}. Planktonic organisms, whether swimming or buoyancy controlled, must

Please cite this article as: Wang, Z., Goodman, L., The evolution of a thin phytoplankton layer in strong turbulence. Continental Shelf Research (2009), doi:10.1016/j.csr.2009.08.006

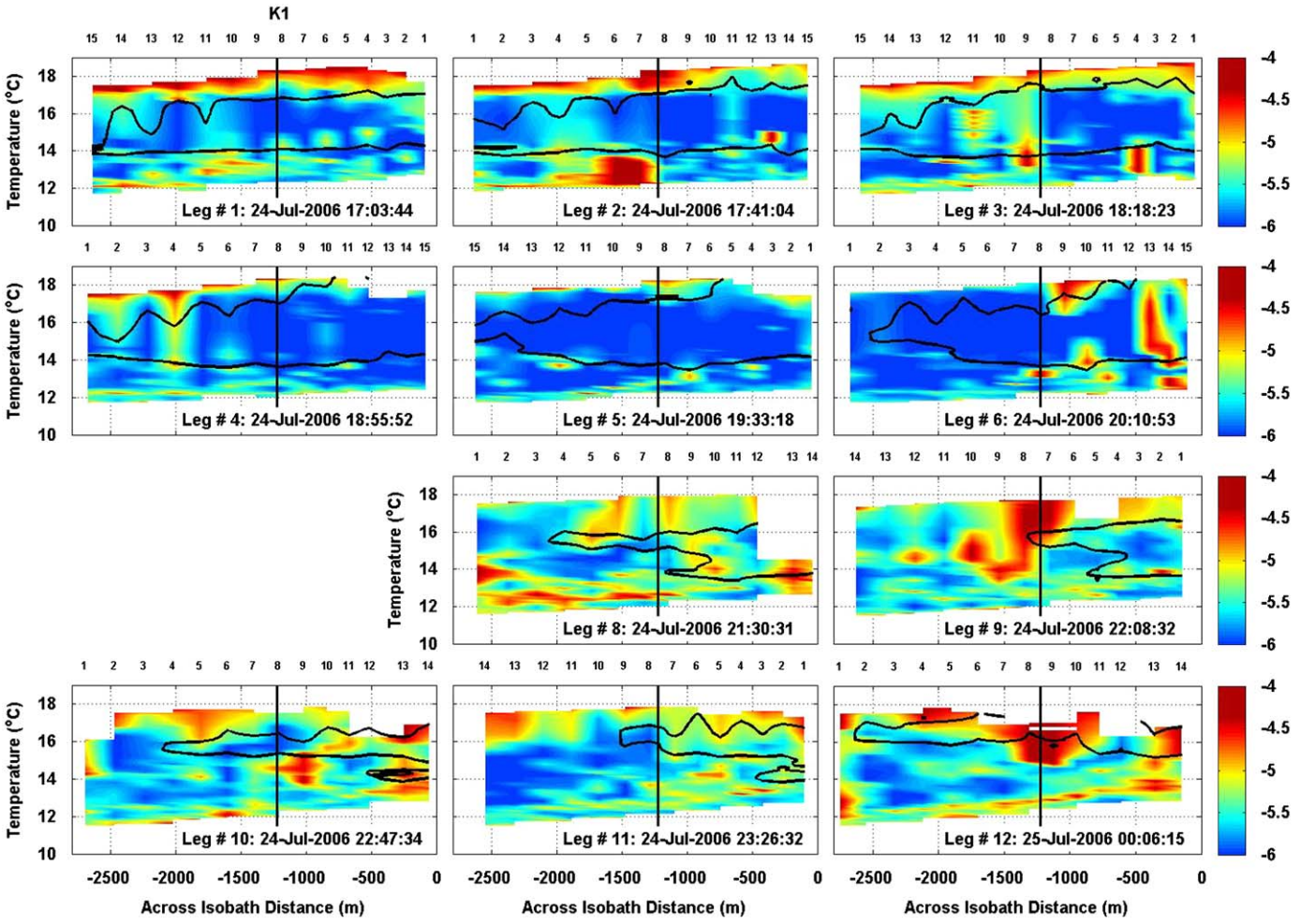

Fig. 7. Contour maps of the turbulent eddy diffusivity, $\log_{10}(\kappa_\rho)$ $m^2 s^{-1}$, using temperature in place of depth as the ordinate. Black contour lines outline thin layers, defined by the criteria used in Section 4.

move at speed $w \gg w_e$ to overcome the effect of being entrained by drag forces into the turbulent field. If $w \ll w_e$, then particles will follow the turbulent field in the manner of a passive Lagrangian tracer.

In Fig. 8 we show contour plots of w_e versus along isobath range and temperature. In the thin layer region between $T = 14$ and 17.4 °C the first half of the experiment was typically characterized by $w_e < 10^{-3}$ m s^{-1} with the exception of a few isolated regions. In the second half of the experiment starting at 21:30 PDT in panel #8, there is a significant increase in regions between $T = 14$ and 17.4 °C where $w_e > 10^{-3}$ m s^{-1}. Note, from Fig. 4, that during the first half of the experiment the largest values of chlorophyll *a* concentration are sharply confined to the upper thermocline layer, marked by the two white line isotherm boundaries $T = 14$ and 17.4 °C. However in the second half of the experiment, Fig. 4 shows chlorophyll *a* concentrations crossing the lower boundary at $T = 14$ °C and becoming more diffuse. From Figs. 6–8, the most intense turbulence in the upper thermocline occurs at the most shoreward locations of the experimental site where we see the largest dispersion effects on the thin layer in Fig. 4.

In order to examine the role of turbulent diffusion on thin layer evolution, we need to use criterion Eq. (8) to identify regions where planktonic organisms act as passive Lagrangian tracers. On July 23 2006, one day before the T-REMUS experiment, results from in situ water sampling (Rines et al., this issue) showed that the major species in the thin layer at the experimental site was the diatom *Chaetoceros concavicornis,* which is non-swimming. Let us assume that such organisms can only move due to changes in its buoyancy with its buoyancy forcing and drag given in the manner discussed in Section 3. From Eqs. (4) and (5) we can use the criterion $(\mathrm{CND}^2/\nu) < 0.1$ which with an observed upper bound N of $N = 3 \times 10^{-2}$ s^{-1} and the upper bound value of $C = 1/4$ results in the constraint that particles diameter satisfy $D < 3$ mm, which, according to Rines (personal communication) is expected to be strongly satisfied at the depth range of observations reported here. Note that for the case of buoyancy control the above criterion depends directly on w_e but not the turbulence strength parameter, Re_b.

There was also some evidence of a fast swimming species phototrophic ciliate *Myrionecta rubra* observed at the LOCO site with swimming speeds ranging from 5 to 9 mm s^{-1} but this organism was entirely confined to the very upper layer at the surface (Rines et al., this issue). In the case of phytoplankton cells sinking (including both growing and senescence), Smayda (1970) has estimated speeds from under 10^{-5} to about 3×10^{-4} m s^{-1}, the upper limit of which is still an order of magnitude less than the turbulent eddy velocity occurring in the second half of the experiment in the region of chlorophyll *a* dispersion.

We thus conclude that during the second half of the 24 July 2006 experiment, during which time strong turbulence occurred in the region between $T = 17.4$ and 14 °C, turbulence will both

Please cite this article as: Wang, Z., Goodman, L., The evolution of a thin phytoplankton layer in strong turbulence. Continental Shelf Research (2009), doi:10.1016/j.csr.2009.08.006

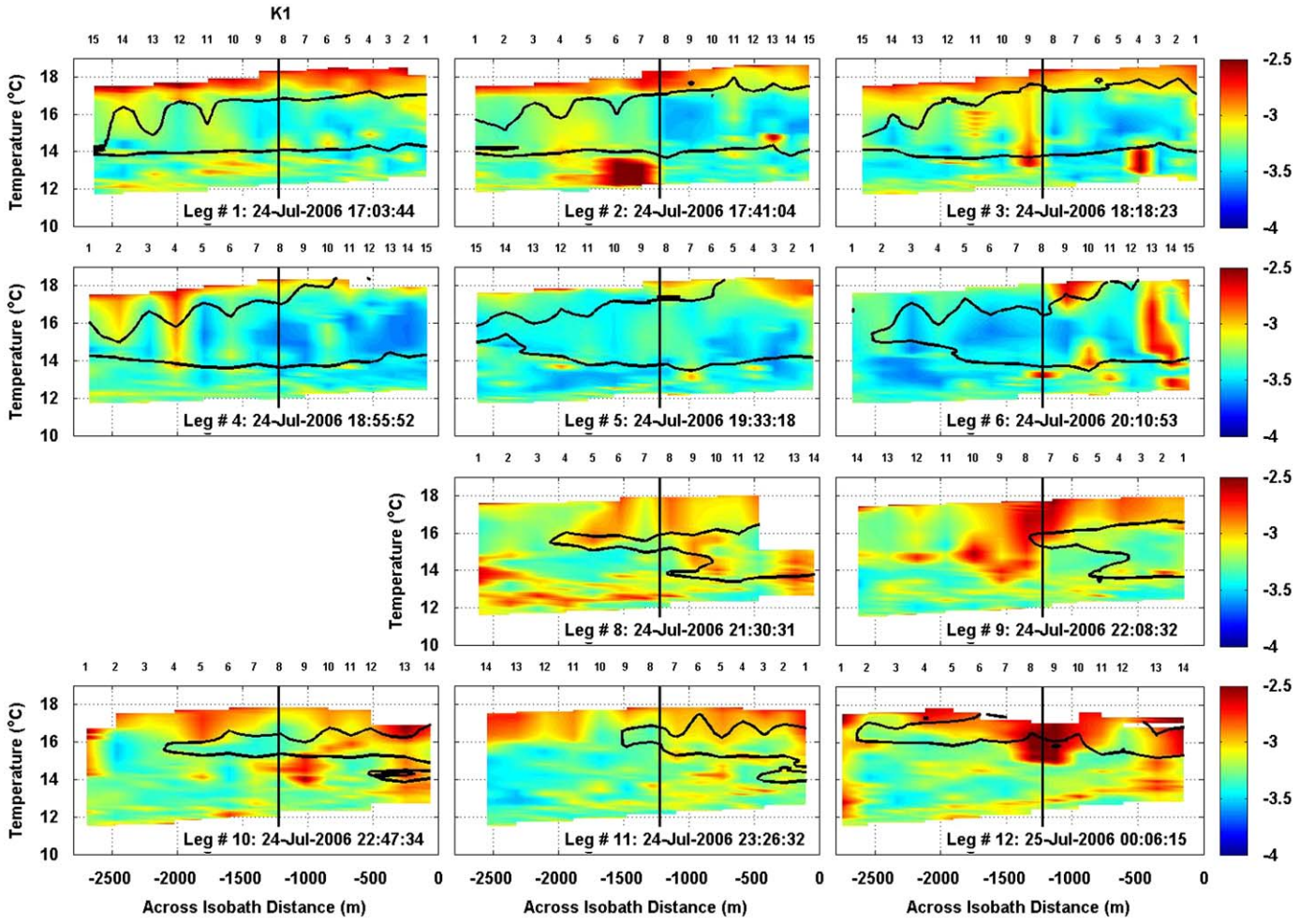

Fig. 8. Contour maps of the turbulent velocity ($m\,s^{-1}$), using temperature in place of depth as the ordinate. Black contour lines outline thin layers, defined by the criteria used in Section 4.

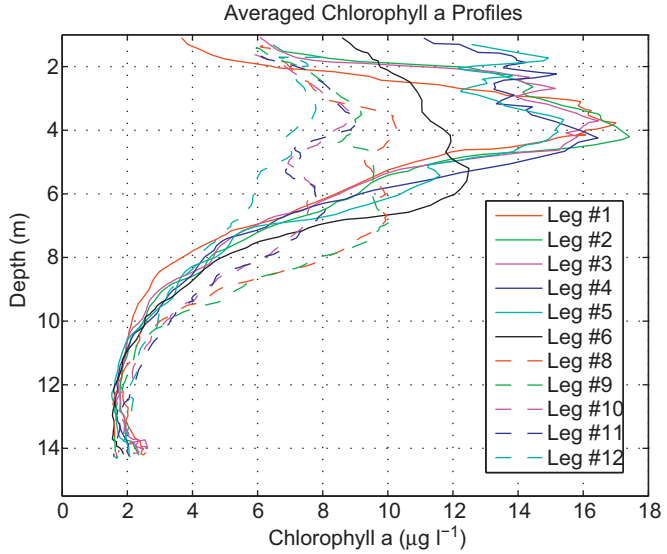

Fig. 9. Averaged vertical profiles of the thermocline chlorophyll *a* thin layer, using the four most onshore profiles. A "stretched" vertical coordinate, based on the average isotherm depth over the experimental region, is used for depth. Profiles from Legs #1–6 are in solid lines and those from Legs #8–12 in dashed lines.

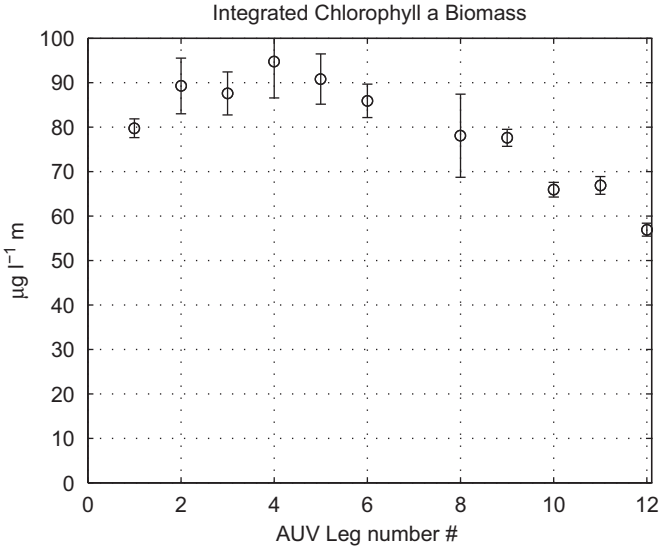

Fig. 10. Vertically integrated chlorophyll *a* biomass of those profiles in Fig. 9. Shown are the one standard deviation (67%) error bars.

entrain and diffuse the diatoms. In the first half of the experiment turbulence was sufficiently weak that, although organisms may have undergone turbulent entrainment, little diffusion occurred.

To examine the evolution of plankton in the region of the strongest turbulence, we plot in Fig. 9 the average of the four most shoreward vertical profiles of chlorophyll *a*, i.e. those between $x = 0$ and -600 m. The vertical axis is a stretched coordinate (Wang and Goodman, 2009), obtained by using the average depth

Please cite this article as: Wang, Z., Goodman, L., The evolution of a thin phytoplankton layer in strong turbulence. Continental Shelf Research (2009), doi:10.1016/j.csr.2009.08.006

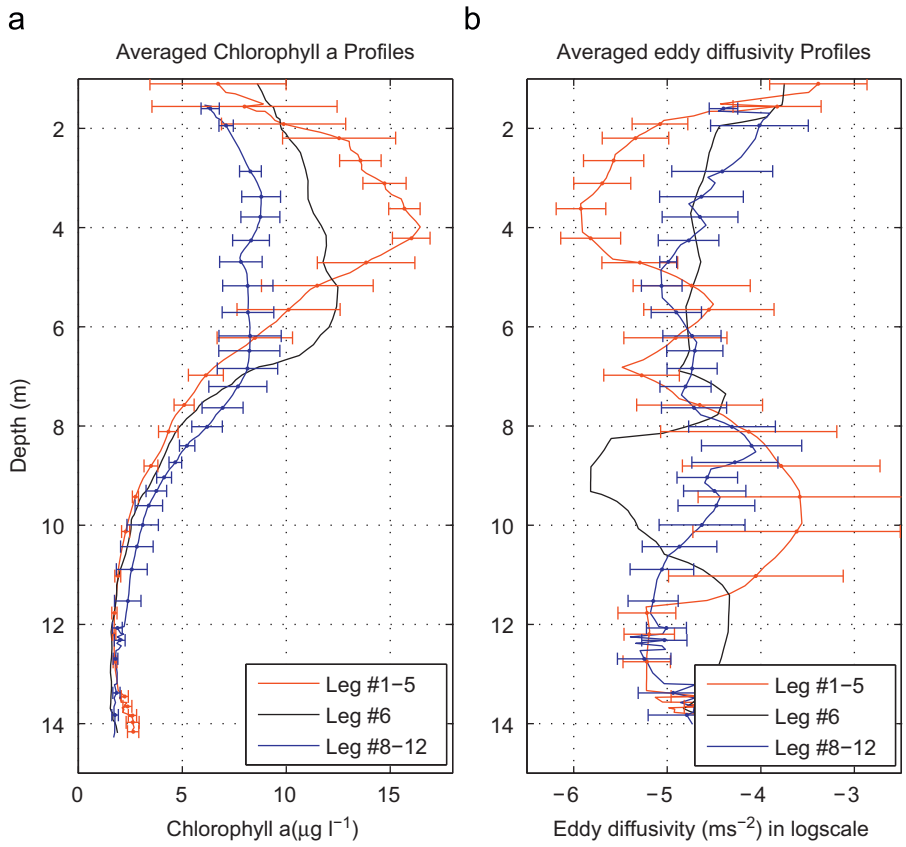

Fig. 11. Profiles of (a) averaged chlorophyll *a* and (b) averaged eddy diffusivity, κ_ρ for Legs #1–5 (red) and 8–12 (blue) in Fig. 9. Profile of Leg #6 was plotted separately (black). The one standard deviation bars are presented for the averaged profiles to indicate their rms variance about the mean. (For interpretation of the references to colour in this figure legend, the reader is referred to the web version of this article.)

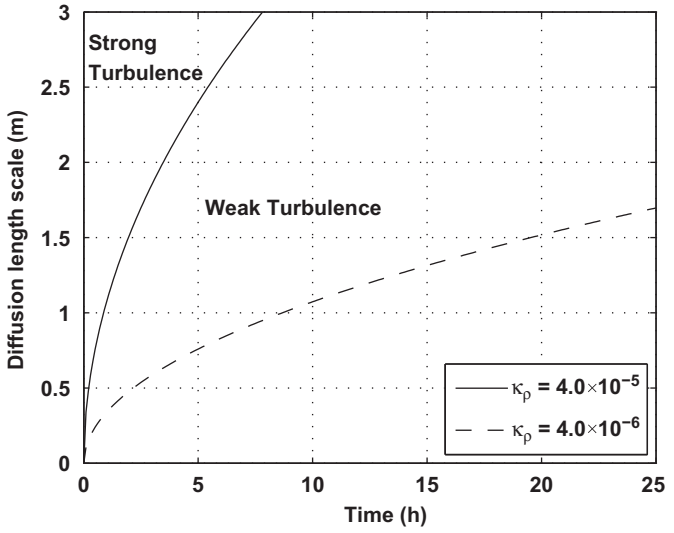

Fig. 12. The characteristic vertical (cross isopycnal) diffusive length scale, $l = 2\sigma$, where $\sigma^2 = 2\kappa_\rho t$ versus time, *t*.

of the isotherms between $T = 17.4$ and 12.2 °C, the depth range of the boundaries of upper and lower thermocline. Similar to using the temperature as the ordinate this vertical coordinate minimizes the distorting effect of internal waves. The profiles from Legs#1–6 are plotted in color-coded solid lines and the profiles from Legs#8–12 in color-coded dashed lines. Because of the type of track performed by the T-REMUS AUV these profiles are not equally spaced in time. Profile pairs (2, 3), (4, 5), (8, 9), and (10, 11) are approximately 7 min apart, while (1, 2), (3, 4), (5, 6), (9, 10), and (11, 12) are 80 min apart. Profiles #6 and 8 are about 85 min apart. Clearly there are three groupings of these profiles. Profiles of Legs #1–5 show a strong large peak in the chlorophyll *a* concentration, centered at 4 m depth and of order 1 m in thickness. Profile #6 shows significant broadening and deepening, a trend which continues with profiles #7–12.

It should be noted that, since the T-REMUS track lines are essentially spatially coincident (within a total along isobath distance of 330 m from tracks 1 to 12), a time series of profile plots such as that displayed in Fig. 9 do not represent samples obtained from the same water mass. Since, on average, the current direction is along isobath (see Figs. 2a and b), using an average along isobath advection velocity of 0.15 m s^{-1}, the water mass which passes the initial part of the first track is approximately 4.0 km downstream from that which crosses the end of the last track, approximately 8 h later. Thus, care should be taken in comparing each of these profiles in that they represent properties within the sampled water mass separated in both space and time.

In Fig. 10 we plot the vertically integrated chlorophyll *a* concentration of these profiles. From Figs. 9 and 10 the chlorophyll *a* profiles of Legs #1–5 are very similar and have a small variation in the integrated chlorophyll *a* content. The Leg #6 profile in Fig. 9, the black curve, is much different than the first five profiles, with a deeper maximum and more diffuse. However its total integrated concentration is, within the level of uncertainty, the same as that of Legs #2–5 profiles. The total vertically integrated chlorophyll *a* content of profiles of Legs #8–12 decrease with time (upstream location) suggesting spatial inhomogeneity of the chlorophyll *a* field in the along isobath direction which commenced after the

Please cite this article as: Wang, Z., Goodman, L., The evolution of a thin phytoplankton layer in strong turbulence. Continental Shelf Research (2009), doi:10.1016/j.csr.2009.08.006

time (upstream location) of profile 6. In Fig. 11 we cluster and present the average of profiles of Legs #1–5 and 8–12 for chlorophyll a (Fig. 11a) and the diffusivity, κ_ρ (Fig. 11b). We plot the profile of Leg #6 separately. The one standard deviation bars are presented for the averaged profiles to indicate their rms variance about the mean. Clearly chlorophyll a profiles in the depth range of the thin layers for the first half of the experiment are characterized by weak turbulence $\kappa_\rho \lesssim 4\times10^{-6}\,\mathrm{m^2\,s^{-1}}$. During the second half of the experiment there is a significant increase in the eddy diffusivity of about an order of magnitude with $\kappa_\rho \gtrsim 4\times10^{-5}\,\mathrm{m^2\,s^{-1}}$, the value at the strong turbulent boundary.

In Fig. 12 we show a plot of the characteristic vertical (cross isopycnal) diffusive length scale, $l=2\sigma$ where $\sigma^2=2\kappa_\rho t$ versus time, t. Usage of this expression for a vertical diffusive length scale neglects any vertical (cross isopycnal) strain rate effects, but not vertical shear effects. (Vertical shear and vertical turbulent diffusion can result in horizontal diffusion, so-called shear dispersion, Young et al., 1982.) It is assumed that the vertical strain rate, β satisfies the condition $\beta=(\partial w/\partial z)\ll(\kappa_\rho/l^2)$. Significant values of β can lead to balance between vertical convergence and vertical diffusion as noted by Stacey et al. (2007). Fig. 12 shows that thin layers of thickness 0.5 m and more under weak turbulent conditions and no vertical convergent strain rate should persist for several hours. The thickest ones >2.0 m would persist for more than a day. Fig. 12 indicates that for strong turbulence a 1.0 m thick thin layer would disperse with $2\sigma=1.0$ m in 1 h. This result is consistent with what is evolving in the second half of the experiment and the lack of the sharp peak of width of order 1.0 m which was present in profiles #1–5 but not in profiles #6 and 8–12 in Fig. 9.

6. Summary and conclusions

A field experiment has been conducted to study the effect of turbulence on the evolution of a thin phytoplankton layer. The experiment occurred in the northern bight of Monterey Bay, CA, USA, on the evening of July 24, 2006 and was part of the "Layered Organization in the Coastal Ocean" (LOCO) 2006 experiment. The AUV T-REMUS was deployed to run in a 5° yo-yo mode. This resulted in turbulence being sampled with a spatial vertical resolution of 0.5 m and an average horizontal resolution of 150 m. Optical and fine scale sampling had the same horizontal resolution but with a 0.1 m vertical resolution. Vehicle depth range extended from 1.0 m below the surface to 4.0 m above the bottom. This depth range covered the location of all of the major physical features present at the LOCO site, i.e. surface layer, thermocline region, and bottom layer. The vehicle was run for 8 h and performed 12 across isobath tracks parallel to the K-line, where other LOCO investigators had set fixed moored and profiling instruments. T-REMUS sensor suite allow the direct, local, and simultaneous measurements of the TKE dissipation rate, ε, the local buoyancy frequency, N, along with chlorophyll a and optical scattering at 470 and 700 nm. The fine and microstructure physical measurements then can be used to estimate three interrelated turbulence parameters of direct relevance to thin layer evolution. These are: the buoyancy Reynolds number, Re_b, the turbulent eddy diffusivity, $\kappa_\rho=\Gamma\nu\mathrm{Re}_b$, and the turbulent eddy velocity, w_e. We find that the boundary value of $\kappa_\rho=4\times10^{-5}\,\mathrm{m^2\,s^{-1}}$ separates weak from strong turbulence.

Estimation of the turbulent eddy velocity, w_e, is critical in assessing whether the turbulent field is intense enough to sweep up biologically based particles and embed them in its flow. We develop a model of phytoplankton response as a Stokes particle. This is then used to determine the criteria when phytoplankton can be considered as a passive Lagrangian tracer. Using the criteria set forth in Section 3 we examine 24 July 2006 T-REMUS data which show a compact spatially contiguous thin phytoplankton layer being advected through the experimental site. The thin layer had an across isobath length of at least 2.5 km and an along isobath length of at least 4 km. It lasted for more than 8 h.

In the first 4 h of observation, weak turbulence was measured within the thin layer, characterized by turbulent eddy diffusivity $\kappa_\rho<4\times10^{-6}\,\mathrm{m^2\,s^{-1}}$ (corresponding to $\mathrm{Re}_b<20$), and turbulent eddy velocity $w'<3\times10^{-4}\,\mathrm{m\,s^{-1}}$. Although distorted by an internal wave train, during this time period the thin layer thickness tended to remain constant. In the second half of the experiment, strong turbulence occurred in the location of the thin layer with the most intense turbulence increasing shoreward. The thin layer changed considerably with its vertical extent decreasing and its concentration weakening. From nearby water sampling on 23 July 2006 (Rines et al., this issue), the dominant species in the thin layer during this time period were shown to be the diatom *C. concavicornis*. It is non-motile, chain-forming and is estimated to satisfy the criterion Eq. (8) for being a passive Lagrangian tracer. During the second half of the experiment the thin layer diffused vertically (across isopycnal) due to the presence of strong turbulence while being advected past the experimental site. Also noted during this time period was a decrease of order 50% in the vertically integrated chlorophyll a content over the depth range where the thin layer occurred. This latter observation could be explained by three factors: (1) horizontal (along isopycnal) diffusion and/or vertical shear straining from the horizontal velocity field of chlorophyll a to outside of the experimental site, (2) the advection of an along isobath spatial gradient of chlorophyll a into the experimental site, (3) the decrease of chlorophyll a material during the along isobath advection from biological processes such as mortality. For factor (1) from Fig. 4, if we use as a characteristic horizontal scale in the second half of the experiment, the across isobath length of 2 km for the thin layer, this would require a horizontal (along isopycnal) diffusivity of $\kappa_h=(\sigma^2/2t)=((2\times10^3\,\mathrm{m})^2/2\times2.5\times3.6\times10^3\,\mathrm{s})=220\,\mathrm{m^2\,s^{-1}}$. It is straightforward to show using our observed data that horizontal diffusivity either from eddy (fluctuating "mean" current) or shear dispersion (Young et al., 1982) would be several orders of magnitude smaller than this value. Vertical shear of the horizontal current field can also distort the shape of a volume of material and result in locations near its edge in a decrease in the vertically integrated chlorophyll a. Following Stacey et al. (2007) (their Fig. 1) if in the plane of motion a rectangularly shaped feature (thin layer) of thickness l, length L, undergoes a vertical shear α over time, t, then it is straightforward to show that on average the fractional change in an observation area $A=lL$ of an initial rectangle, $\Delta A/A$, would be given by $(\Delta A/A)=(\alpha tl/2L)$. For the across isobath direction if we take $L=2.0$ km, a maximum thin layer thickness of $l=3$ m, using the on board ADCP shear during the second half of the experiment of $\alpha=10^{-2}\,\mathrm{s^{-1}}$ then $(\Delta A/A)=0.07$, which is about a factor of 8 smaller for the decrease in the vertically integrated chlorophyll a observed in Fig. 10 during the second half of the experiment. However the observations used in Fig. 10 were located at the most shoreward part of the experimental region and during the ebb cycle. Thus if the chlorophyll a thin layer field abruptly vanished shoreward of the observation location this factor could be increased by as much as $(2000/600\,\mathrm{m})=5$. We do not have data to ascertain factors (2) or (3).

Thus we conclude that strong turbulence played the key role in the across isopycnal diffusion of the thin layer with advection and possibly shear the mechanisms of along isopycnal transport. Biological processes such as sinking may also have been a factor in decreasing the overall content of the thin layer region during the time period of observation.

Please cite this article as: Wang, Z., Goodman, L., The evolution of a thin phytoplankton layer in strong turbulence. Continental Shelf Research (2009), doi:10.1016/j.csr.2009.08.006

Acknowledgements

This work was funded by the ONR Marine Mammals & Biological Oceanography Program, Grant N000140410254, Dr. J. Eckman Program Director, whom we greatly appreciate both for financial support and wise program guidance. We also thank our colleagues D.V. Holliday and M.T. Stacey for providing supporting data from the K1 line thermistor chain and ADCP. Valuable conversations were carried out with J.E.B. Rines and J.M. Sullivan. We thank guest editor J.M. Sullivan and the two anonymous reviewers for their valuable comments and suggestions.

Appendix A. : Modeling phytoplankton as a Stokes particle in a buoyancy field

Consider a particle of density, ρ with $\Delta\rho$ to the local density of the surrounding vertically stratified fluid, moving in the vertical, z, and undergoing forcing by drag, F_D, buoyancy, F_B, and self-propulsion (swimming), F_P. Its motion is then given by

$$(m + m_{added})\frac{d^2z}{dt^2} = F_D + F_B + F_P \qquad (A-1)$$

where m is its mass, and m_{added}, the added mass due to the inertia effects of acceleration in the fluid. If we assume that the Reynolds number of the particle is in the Stokes regime, i.e. $R = (w_{rel}L/\nu) \lesssim 1$, where w_{rel} is the particle velocity relative to the surrounding fluid, L a characteristic length scale of the particle, and ν the kinematic viscosity, then F_D can be modeled by a Stokes drag law with $F_D \propto w_{rel}$ (Batchelor, 1994, Lai and Mockros, 1972). Following Stacey et al. (2007) and Franks (1992), for the case of non-propulsive (non-swimming) phytoplankton which adjust their buoyancy to the local environment, we set in Eq. (A-1) $F_P = 0$ and

$$F_B = -\Delta\rho Vg = \rho V N^2 z \qquad (A-2)$$

where N is the background buoyancy frequency, and V its volume whence Eq. (A-1) becomes

$$\frac{d^2z}{dt^2} + \frac{1}{\tau}\frac{dz}{dt} + AN^2 z = 0 \qquad (A-3)$$

where for a spherically shaped particle of diameter D

$$\tau = \tau_s = \frac{D^2}{12\nu} \qquad (A-4a)$$

$$A = A_s = \frac{2}{3} \qquad (A-4b)$$

while for the more general case of an oblate spheroid, i.e. an ellipsoid of revolution of diameter D and length L,

$$\tau = \tau_s = S\frac{D^2}{12\nu} \qquad (A-5a)$$

$$A = A_s = \frac{2}{3}S' \qquad (A-5b)$$

where $S = S(D/L)$, $S' = S'(D/L)$ are shape factors which are a function of the ratio of the minor to major axes and the direction of flow relative to these axes. For flow transverse to the axis of an oblate spheroid $S<1$ and $S'>1$ (Gosh, 1954; Newman, 1977). For the extreme limiting case of a cylindrically shaped particle of length L, diameter D with $L \gg D$ and flow transverse to its axis

$$\tau = \tau_c = C(R)\frac{D^2}{4\nu} \qquad (A-6a)$$

$$A = A_c = \frac{1}{2} \qquad (A-6b)$$

with the constant $C(R) \approx 1$ for $R \approx 1$ (Batchelor, 1994), R the Reynolds number. Note that the implicit assumption in using Eq. (A-2) in Eq. (A-1) for ocean application is that the diatom matches the compressibility and isothermal and isohaline expansion of the background field and that its surface viscosity are sufficiently close to that matches that of the local environment that their effects can be ignored.

If we assume that the particle is initially ($t = 0$) at rest but displaced some distance l from $z = 0$, the solution to Eq. (A-3) is

$$z = \frac{l}{\beta_2 - \beta_1}(\beta_2 e^{-\beta_1 t} - \beta_1 e^{-\beta_2 t}) \qquad (A-7)$$

where $\beta_{1,2}$ satisfies the equation

$$\beta^2 - \frac{\beta}{\tau} + AN^2 = 0$$

This has the solutions

$$\beta = \frac{1}{2\tau}[1 \pm (1 - 4AN^2\tau^2)^{1/2}] \qquad (A-8)$$

Note that if

$$4AN^2\tau^2 \ll 1 \qquad (A-9)$$

$$\beta_1 = \frac{1}{\tau} \qquad (A-10a)$$

$$\beta_2 = AN^2\tau \qquad (A-10b)$$

Using β_1, β_2 in Eq. (A-7) and condition (A-9), for a time t such

$$\frac{1}{AN\tau}N^{-1} \gg t \gg \tau \qquad (A-11)$$

results in

$$\frac{dz}{dt} = w = AlN^2\tau e^{-N^2\tau t} \approx AlN^2\tau \qquad (A-12)$$

Note from Eq. (A-11) that Eq. (A-12) is valid over the buoyancy time period $N^{-1}$and gives the maximum velocity the particle would achieve under constraint (A-9).

Now consider the case where the fluid itself moves either due to phenomena such as turbulence or internal waves, then both the drag force term and the buoyancy terms of Eq. (A-1) should reflect that particle motion be taken relative to the fluid, whence Eq. (A-3) becomes

$$\frac{d^2z}{dt^2} + \frac{1}{\tau}\left(\frac{dz}{dt} - \frac{dz_T}{dt}\right) + AN^2(z - z_T) = 0 \qquad (A-13)$$

where z_T, is the displacement of the flow field from the equilibrium position at $z = 0$. Because the fluid now exerts drag and buoyancy forcing on the particle let us rewrite Eq. (A-13) in the form of a forced damped harmonic oscillator namely,

$$\frac{d^2z}{dt^2} + \frac{1}{\tau}\frac{dz}{dt} + AN^2 z = f(t) \qquad (A-14)$$

where

$$f(t) = f_T(t) = \frac{w_T}{\tau} + AN^2 z_T \qquad (A-15)$$

with $w_T = (dz_T/dt)$.

Eq. (A-14) has forced and free solutions. One particular free solution (boundary conditions $z = 1$, $w = 0$ at $t = 0$) is given by Eq. (A-7). The forced solution is given by

$$z = -\int_0^t dt' \frac{f(t')}{\beta_2 - \beta_1}[e^{-\beta_2(t-t')} - e^{-\beta_1(t-t')}] \qquad (A-16)$$

Finally for the case of phytoplankton having self-propulsion we would include a propulsive forcing term on the right hand side of Eq. (A-15).

$$f(t) = f_P(t) + f_T(t) \qquad (A-17)$$

Please cite this article as: Wang, Z., Goodman, L., The evolution of a thin phytoplankton layer in strong turbulence. Continental Shelf Research (2009), doi:10.1016/j.csr.2009.08.006

References

Alldredge, A.L., Cowles, T.J., MacIntyre, S., Rines, J.E.B., Donaghay, P.L., Greenlaw, C.F., Holliday, D.V., Dekshenieks, M.M., Sullivan, J.M., Zaneveld, J.R.V., 2002. Occurrence and mechanisms of formation of a dramatic thin layer of marine snow in a shallow Pacific fjord. Marine Ecology Progress Series 233, 1–12.

Baines, P.G., 1986. Internal tides, internal waves and near-inertial motions. In: Mooers, C.N.K. (Ed.), Baroclinic Processes on Continental Shelves. American Geophysical Union, Washington, DC, pp. 19–31.

Batchelor, G.K., 1994. An Introduction to Fluid Dynamics. Cambridge university press, Cambridge.

Bogucki, D., Dickey, T., Redekopp, L.G., 1997. Sediment resuspension and mixing by resonantly generated internal solitary waves. Journal of Physical Oceanography 27, 1181–1196.

Breaker, L.C., Broenkow, W.W., 1994. The circulation of Monterey Bay and related processes. Oceanography and Marine Biology: An Annual Review 32, 1–64.

Carter, G.S., Gregg, M.C., Lien, R.C., 2005. Internal waves, solitary-like waves, and mixing on the Monterey Bay shelf. Continental Shelf Research 25 (12–13), 1499–1520.

Dekshenieks, M.M., Donaghay, P.L., Sullivan, J.M., Rines, J.E.B., Osborn, T.R., Twardowski, M.S., 2001. Temporal and spatial occurrence of thin phytoplankton layers in relation to physical processes. Marine Ecology Progress Series 223, 61–71.

Donaghay, P.L., Rimes, H.M., Sieburth, J.M., 1992. Simultaneous sampling of fine scale biological, chemical and physical structure in stratified waters. Archiv für Hydrobiologie Beiheft Ergebnisse der Limnologie 36, 97–108.

Franks, P.J.S., 1992. Sink or swim-accumulation of biomass at fronts. Marine Ecology Progress Series 82, 1–12.

Gargett, A.E., Osborn, T.R., Nasmyth, P.W., 1984. Local isotropy and the decay of turbulence in a stratified fluid. Journal of Fluid Mechanics 144, 231–280.

Goodman, L., Levine, E.R., Lueck, R.G., 2006. On measuring the terms of the turbulent kinetic energy budget from an AUV. Journal of Atmospheric and Oceanic Technology 23, 977–990.

Goodman, L., Wang, Z., 2009. Turbulence observations in the northern bight of Monterey Bay from a small AUV. Journal of Marine Systems: Special Issue on marine turbulence 77 (4), 441–458.

Gosh, N.L., 1954. Resistance in potential flow: prolate and oblate spheroids. Proceedings of the National Institute of Sciences of India 20, 74–103.

Gregg, M.C., 1987. Diapycnal mixing in the thermocline: a review. Journal of Geophysical Research 92 (C5), 5249–5286.

Holliday, D.V., Pieper, R.E., Greenlaw, C.F., Dawson, J.K., 1998. Acoustical sensing of small scale vertical structures in zooplankton assemblages. Oceanography 11 (1), 18–23.

Istweire, E.C., Koseff, J.R., Briggs, D.A., Ferziger, J.H., 1993. Turbulence in stratified shear flows: implications for interpreting shear-induced mixing in the oceans. Journal of Physical Oceanography 23, 1508–1522.

Kamykowshi, D., 1995. Review: trajectories of autotrophic marine dinoflagellates. Journal of Phycology 31, 200–208.

Kunze, E., Rosenfeld, L.K., Carter, G.S., Gregg, M.C., 2002. Internal waves in Monterey Submarine Canyon. Journal of Physical Oceanography 32 (6), 1890–1913.

Lai, R.Y.S., Mockros, L.F., 1972. The Stokes-flow drag on prolate and oblate spheroids during axial translatory accelerations. Journal of Fluid Mechanics 52 (1), 1–15.

Luketina, D.A., Imberger, J., 2001. Determining turbulent kinetic energy dissipation from Batchelor curve fitting. Journal of Atmospheric and Oceanic Technology 18 (1), 100–113.

Mann, K.H., Lazier, J.R.N., 2006. Dynamics of Marine Ecosystems: Biological–Physical Interactions in the Oceans, third ed. Blackwell publishing, MA, USA.

MacDonald, D.G., Goodman, L., Hetland, R.D., 2007. Turbulent dissipation in a near field river plume: a comparison of control volume and microstructure observations with a numerical model. Journal of Geophysical Research 112, C07026, doi:10.1029/2006JC004075.

McManus, M.A., Alldredge, A.L., Barnard, A., Boss, E., Case, J., Cowles, T.J., Donaghay, P.L., Eisner, L., Gifford, D.J., Greenlaw, C.F., Herren, C., Holliday, D.V., Johnson, D., MacIntyre, S., McGehee, D., Osborn, T.R., Perry, M.J., Pieper, R., Rines, J.E.B., Smith, D.C., Sullivan, J.M., Talbot, M.K., Twardowski, M.S., Weidemann, A., Zaneveld, J.R.V., 2003. Changes in characteristics, distribution and persistence of thin layers over a 48-h period. Marine Ecology Progress Series 261, 1–19.

McManus, M.A., Cheriton, O.M., Drake, P.J., Holliday, D.V., Storlazzi, C.D., Donaghay, P.L., Greenlaw, C.F., 2005. The effects of physical processes on the structure and transport of thin zooplankton layers in the coastal ocean. Marine Ecology Progress Series 301, 199–215.

Moum, J.N., Farmer, D.M., Smyth, W.D., Armi, L., Vagle, S., 2003. Structure and generation of turbulence at interfaces strained by internal solitary waves propagating shoreward over the continental shelf. Journal of Physical Oceanography 33, 2093–2112.

Nahon, M., 1996. A simplified dynamics model for autonomous underwater vehicles. Autonomous Underwater Vehicle Technology, AUV 96, 373–379.

Newman, J.N., 1977. Marine Hydrodynamics. MIT press, Cambridge, MA.

Osborn, T.R., 1980. Estimates of the local rate of vertical diffusion from dissipation measurements. Journal of Physical Oceanography 10, 83–89.

Park, M.G., Cooney, S.K., Kim, J.S., Coats, D.W., 2002. Effects of parasitism on diel vertical migration, phototaxis/geotaxis, and swimming speed of the bloom-forming dinoflagelalte Akashiwo sanguinea. Aquatic Microbial Ecology 29, 11–18.

Rines, J.E.B., McFarland, M., Donaghay, P.L., Sullivan, J.M., 2009. Thin layers and species-specific characterization of the phytoplankton community in Monterey Bay, California USA. Continental Shelf Research, this issue.

Rothschild, B.J., Osborn, T.R., 1988. Small-scale turbulence and plankton contact rates. Journal of Plankton Research 10, 465–474.

Sander, J., Simon, A., Jonas, T., Wuest, A., 2000. Surface turbulence in natural waters: a comparison of large eddy simulations with microstructure observations. Journal of Geophysical Research 105, 1195–1207.

Shea, R.E., Broenkow, W.W., 1982. The role of internal tides in the nutrient enrichment of Monterey Bay, California. Estuarine, Coastal and Shelf Science 15, 57–66.

Sherman, J.T., Davis, R.E., 1995. Observations of temperature microstructure in NATRE. Journal of Physical Oceanography 25, 1913–1929.

Smayda, T.J., 1970. The suspension and sinking of phytoplankton in the sea. Oceanography and Marine Biology: An Annual Review 8, 353–414.

Stacey, M.T., McManus, M.A., Steinbuck, J.V., 2007. Convergences and divergences and thin layer formation and maintenance. Limnology and Oceanography 52, 1523–1532.

Sullivan, J.M., Swift, E., 2003. Effects of small-scale turbulence on net growth rate and size of ten species of marine dinoflagellates. Journal of Phycology 39, 83–94.

Sullivan J.M., Donaghay, P.L., Rines, J.E.B., 2009. Coastal thin layer dynamics: consequences to biology and optics. Continental Shelf Research, this issue, doi:10.1016/j.csr.2009.07.009.

Tennekes, H., Lumley, J.L., 1972. A First Course in Turbulence. The MIT Press, Cambridge, MA.

Thorpe, S.A., 2005. The Turbulent Ocean. Cambridge University Press, New York, USA.

Wang, Z., Goodman, L., 2009. Evolution of the spatial structure of a thin phytoplankton layer into a turbulent field. Marine Ecology Progress Series 374, 57–74, doi:10.3354/meps07738.

Yamazaki, H., Osborn, T., 1990. Dissipation estimates for stratified turbulence. Journal of Geophysical Research 95, 9739–9744.

Young, W.R., Rhines, P.B., Garrett, C.J.R., 1982. Shear-flow dispersion, internal waves and horizontal mixing in the ocean. Journal of Physical Oceanography 12, 515–527.

Please cite this article as: Wang, Z., Goodman, L., The evolution of a thin phytoplankton layer in strong turbulence. Continental Shelf Research (2009), doi:10.1016/j.csr.2009.08.006